Calhoun
Institutional Archive of the Naval Postgraduate School

Calhoun: The NPS Institutional Archive

DSpace Repository

Theses and Dissertations | 1. Thesis and Dissertation Collection, all items

1971

Sound dispersion and phase fluctuations in the upper ocean.

Rautmann, Jürgen.

Monterey, California ; Naval Postgraduate School

http://hdl.handle.net/10945/15906

Downloaded from NPS Archive: Calhoun

http://www.nps.edu/library

Calhoun is the Naval Postgraduate School's public access digital repository for research materials and institutional publications created by the NPS community. Calhoun is named for Professor of Mathematics Guy K. Calhoun, NPS's first appointed -- and published -- scholarly author.

Dudley Knox Library / Naval Postgraduate School
411 Dyer Road / 1 University Circle
Monterey, California USA 93943

SOUND DISPERSION AND PHASE FLUCTUATIONS IN THE UPPER OCEAN

Jürgen Rautmann

NAVAL POSTGRADUATE SCHOOL
Monterey, California

THESIS

SOUND DISPERSION AND PHASE FLUCTUATIONS

IN THE UPPER OCEAN

by

Jürgen Rautmann

Thesis Advisor: H. Medwin

December 1971

Approved for public release; distribution unlimited.

Sound Dispersion and Phase Fluctuations in the Upper Ocean

by

Jürgen Rautmann
Kapitanleutnant, Federal German Navy

Submitted in partial fulfillment of the
requirements for the degree of

MASTER OF SCIENCE IN ENGINEERING ACOUSTICS

from the

NAVAL POSTGRADUATE SCHOOL
December 1971

R 2454
c.1

ABSTRACT

In-Situ measurements of the speed of sound in the upper ocean have revealed the existence of significant dispersion and large fluctuations over the frequency range 25-80 kHz. The near-surface values of c ranged from +6 M/sec to -3 M/sec relative to the bubble-free value, with a maximum estimated error of 0.5 M/sec. It was possible to identify bubbles of "surface" radius centered around 54 microns down to 4.3 meter depth as well as a population centered around 124 microns (at 4.3 M) found at all depths. The speed fluctuation showed near-Gaussian probability density functions except at the dispersion center frequencies. The standard deviation of the speed varied from 0.27 M/sec for 58.0 kHz to 0.52 M/sec at 69.6 kHz. The phase remained temporally correlated only for 1.46 sec., which was very close to the correlation times of the oceanographic variables. The power spectral density of the varying phase showed its strongest values at frequencies less than 0.5 Hz.; this was presumably due to bubbles entrained at orbital frequencies associated with the surface wave system which had maximum energy in the same frequency range.

TABLE OF CONTENTS

ACKNOWLEDGEMENTS

The writer highly appreciates the guidance and assistance by Professor Herman Medwin of the Physics Department, U. S. Naval Postgraduate School in this research work. Thanks are also due to Mr. William Smith of the USNPGS for his help in the construction and acquisition of equipment. In addition the writer wants to thank Mrs. Pimporn Zeleny for her assistance in working out the computer program No. 3.

The writer is also indebted to the personnel of the U. S. Navy Undersea Research and Development Center and in particular to Mr. Dale Good. This research work was supported by Naval Ship Systems Command.

I. INTRODUCTION

The objective of this research was to take in-situ acoustical measurements in the surface layer of the ocean in order to determine the existence of dispersion and fluctuations of the speed of sound. The anticipated source of frequency-dependent speed of sound in sea-water are bubbles, of various radii, of numbers dependent on the depth. A knowledge of this dispersive behaviour is of importance for sound propagation in near-surface ducts where a change in the speed of sound with depth would result in a change in the refraction of the sound ray. If bubbles exist near the sea surface a sound ray would bounce more often from the surface over a constant horizontal distance as compared with the bubble-free case.

The problem has already been treated in theory as in the analysis worked out by Meyer and Skudrzyk (1950). Fox, Curley and Larson have examined in the laboratory environment the phase velocity in water containing a high density of air bubbles (1954). Glotov et al. (1962) studied a population of bubbles generated by wind-agitated breaking waves in a laboratory tank. Of the few known data actually taken in the ocean those given by Buxcey et al. (1965) and analyzed in the open literature by Medwin (1970) will be referenced here.

Since virtually no in-situ ocean measurements of bubble effects were available, this research was proposed and carried out using the U. S. Navy Undersea Research and Development Center (NUC) Oceanographic Research Tower in Mission Bay/San Diego as a test platform.

A stable, accurately known, continuous wave acoustical signal was received by two spatially separated hydrophones mounted on the sound

axis and their output was compared in phase by means of a digital phase meter. The phase difference between the two hydrophones was recorded at each frequency. The frequency was incremented in steps of approximately two or four kHz over a range from 25 to 80 kHz and for four different water depths. The average results have been interpreted in terms of a change in the speed of sound with frequency at a constant depth, and with depth at a constant frequency. The statistics of the phase change with time have also been calculated.

At the same time, and at the same location, the local sound amplitude modulation due to the spatial and temporal changes in the medium has been examined (thesis by LCDR W. J. Smith, December 1971). In addition, field measurements were taken to determine the fluctuating temperature, salinity, turbulent velocity in x, y, and z-directions, speed of sound as given by a velocimeter and wave height in order to allow a better judgment of the acoustic-oceanic interaction (theses by Lt. M. Bordy, LCDR C. Duchock and Lt. H. Seymour, March 1972).

II. INSTRUMENTATION

A steel-pipe frame shaped like a "square C" of height and length six ft was used to mount the transducer and the hydrophones as shown in Fig. 1. To prevent the frame from acting like a huge tuning fork and thereby displacing the hydrophones, the frame was put under tension halfway down and at the open end by spring-loaded wires. To minimize the reflections from the frame caused by side-lobes of the transducer the upper and lower members were covered with acoustic absorbent rubber (SoAB) at the specular points.

Opposite to the open end of the frame and at the center an USRD F27 unidirectional transducer was mounted. At the sound axis of this transducer an Atlantic Research LC-10 hydrophone was placed 78 cm from the first one and a total of 173 cm from the F27. This distance between the hydrophones was chosen to make the measuring path long enough to measure the effect of the bubbles while at the same time limiting the overall size of the frame.

The transmitting part of the instrumentation (Fig. 2) consisted of the highly stable General Radio Coherent Decade Frequency Synthesizer Type 1162-A generating a sinusoidal voltage of two volts rms and variable in frequency. This signal was then amplified by a Hewlett Packard Power 467A Amplifier to 14.1 V rms and then impressed across the transducer emitting the sound wave. The receiving part of the instrumentation (see Fig. 2) consisted of hydrophone #1 with a sensitivity of -125 dB re 1 volt/microbar and hydrophone #2 with a sensitivity of -106 dB re 1 volt/microbar at 40 kHz which picked up the acoustical signal. The

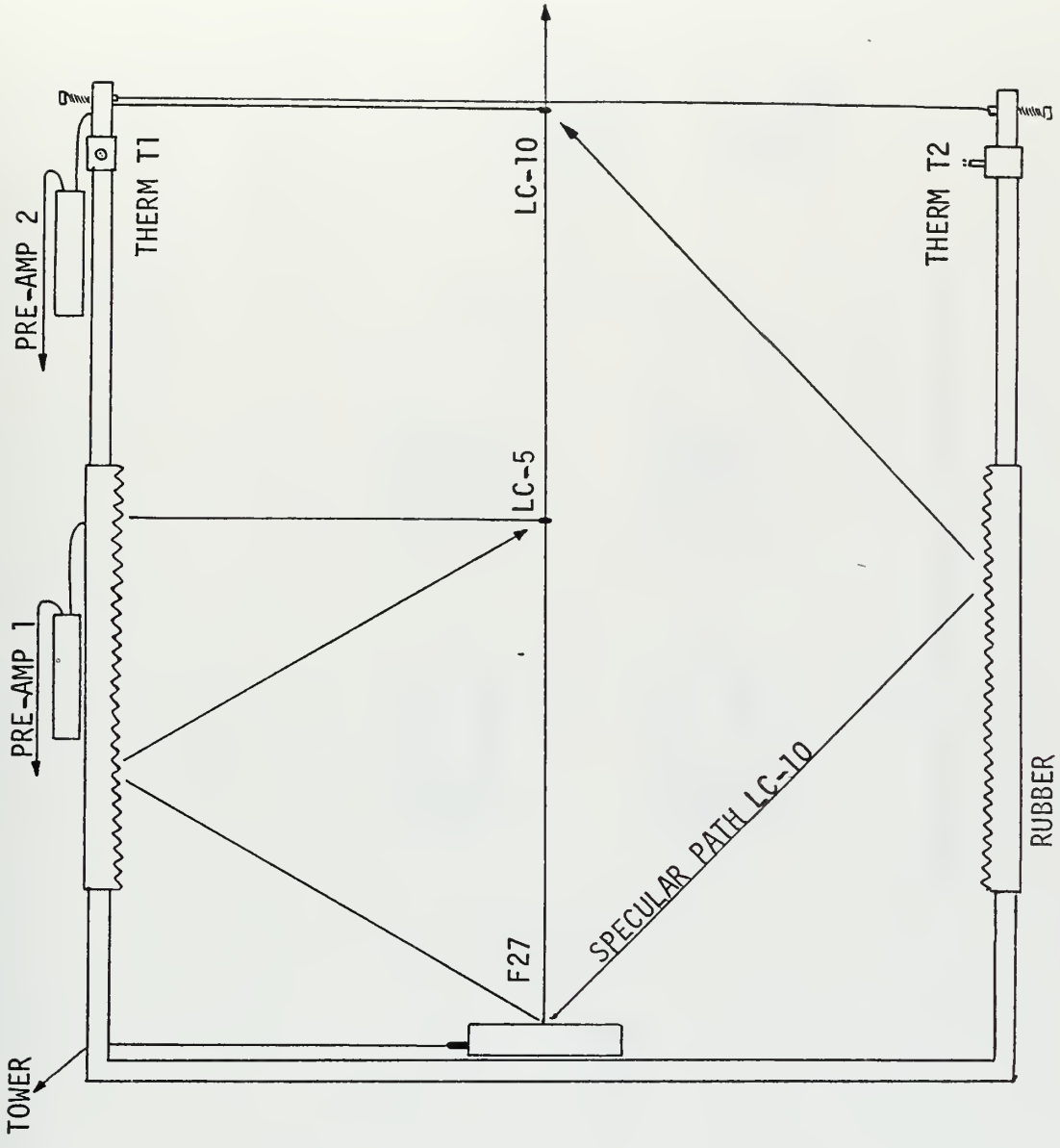

Fig. 1

Mounting of Transducer and Hydrophones

$$C = \frac{fx}{n+\varphi/360}$$

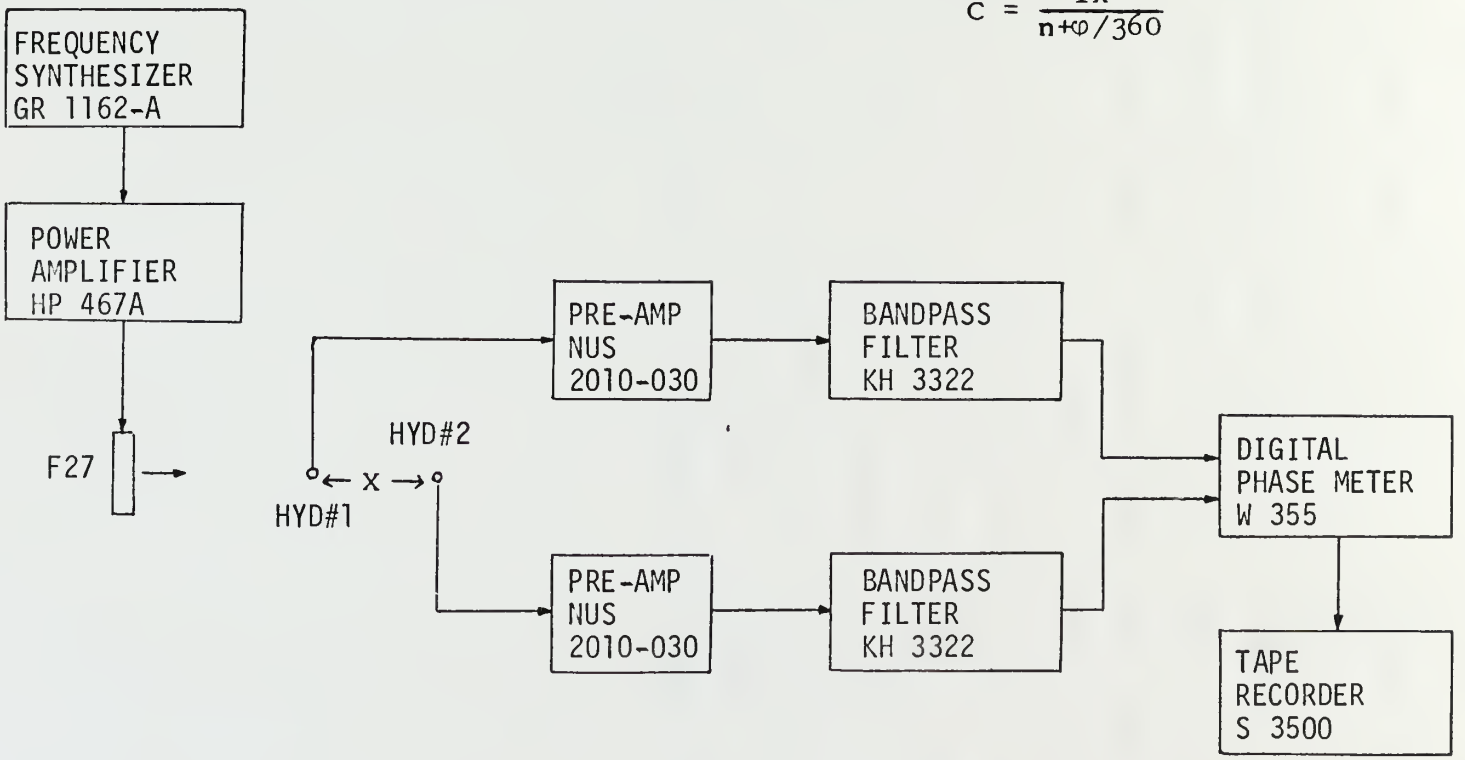

Fig. 2. Transmitting and Receiving Instrumentation

two signals were amplified by 30 dB by an NUS Pre-Amplifier Model 2010-030 before being sent through (150) ft of waterproof shielded cable. Both signals were then bandpass-filtered by a digitally tuned variable Krohn-Hite Model 3322 Filter. The received signal was always bandpass-filtered with the center frequency equal to the frequency of the transmitted signal through a passband of ± 300 Hz, with -48 dB per octave attenuation on either side of the passband. After the Bandpass-Filter the signals were fed into a Wiltron Digital Phase Meter Model 355 which measures the phase angle between the two ac voltages of the same frequency and provides a visual display as well as a dc voltage output proportional to the measured phase angle at 10 mV per degree. This dc voltage was then FM recorded on a Sangamo Model 3500 fourteen track magnetic tape recorder simultaneously with the oceanographic data at a recording speed of 1 7/8 inch per sec. The dynamic range of the recorder utilized was .01 to 2.5 volts, with all the readings falling within this range.

III. OCEANOGRAPHIC COMPONENTS

It was desired to define the volume of water carrying the acoustical signal in terms of the measurable parameters temperature, salinity, particle velocity, speed of sound as given by a velocimeter, and surface wave height. Therefore ocean sensors were mounted close to the acoustic system but not interfering with its performance (see Fig. 3 for geometry). Three thermistors (T1, T2, T3) measured the temporal variation in the temperature, and the temperature probe (T4) of the Bissett-Berman apparatus gave absolute readings between 14° and 19° C. The Bissett-Berman salinometer yielded the temporal variation in the salinity (S) for values ranging from 37.5 to 39.5 ppt. The speed of sound c = c(T, S, depth) was taken by a Ramsey SVTD probe that provided a temporal variation around a DC-value. The particale velocity was obtained with an electromagnetic flowmeter reading one horizontal component (u) or (v) and the vertical component (w). A pressure wave height indicator and a Baylor gauge gave information on the instantaneous wave height.

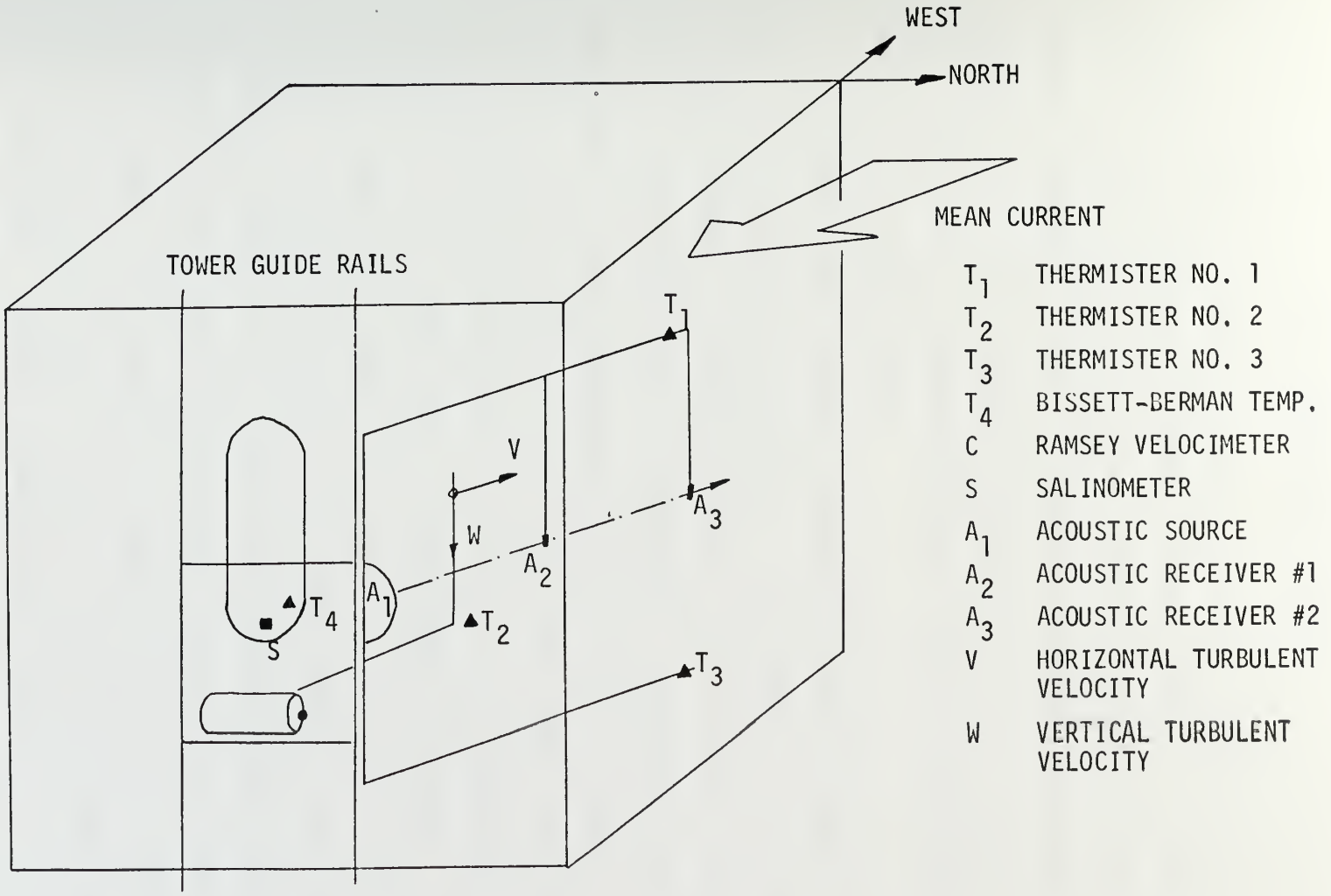

Fig. 3. Spatial Configuration of Acoustic and Ocean Sensors

IV. EXPERIMENTAL SETUP

A continuous wave method was used instead of a pulse-echo system in order to avoid possible errors related to pulse rise time, definition of the leading edge of the pulse, distortion of the pulse when passing through the medium because of frequency-dependent attenuation effects and the difficulty to determine the phase shift on reflection (see Ref. 7). This concern was particularly true since we wanted measurements over a wide frequency range.

The method used to measure the speed of sound is actually derived from a phase interference approach. The frequency of the signal applied to the transducer is adjusted by means of the frequency synthesizer until a wanted phase angle is approached at the output of the digital phase meter. Since the Sangamo recorder required a signal of at least 100 mV and at the same time the digital phase meter is most accurate in its reading for phase angles close to zero, the frequency was always adjusted to get a phase value of approximately 20 degrees. Since the digital phase meter compares the signal at input B with respect to the signal at input A and cannot detect integer number of wave lengths difference between the two signals, the displayed phase determines the fractional wave length by which signal B leads or lags signal A depending on the sign. This means that an integer number of wave lengths plus this fractional part just fits into the separation distance between the two hydrophones. Further increasing the frequency will finally change the phase by 360 degrees or step up the integer number of wave lengths by one and thus produce the next frequency to be recorded.

Because bubble populations were expected to be large in the radius range 40-150 microns we examined the frequency range from 25-80 kHz. The 78. cm separation between the two hydrophones caused the number of wave lengths within this spacing to be incremented by one approximately every two kHz. In order to exclude possible errors in the results due to temporal changes in the medium it was necessary to examine the total frequency range in as short a period of time as possible. Therefore it was decided to accept 20 minutes as an upper limit for stationarity of the medium. The time was also the lower limit to find the frequency spectrum of the ocean wave height and turbulent velocity. This time allowed us to examine the frequency range in steps of four kHz. and to record the time-variable phase difference between the hydrophones for one minute at those frequencies.

In addition to examining the speed of sound with changing signal frequency at a constant depth, readings were taken of the variation of the speed for sound with varying depths at a constant frequency. Four different depths were chosen in order to observe near-surface to near-bottom effects: 4.3, 9.3, 14.3, 7.3 m. These depths were chosen to minimize interference from the underwater beam structure of the tower. The order was picked to decrease and to check on the possibility of longtime variations in the medium. The depths are in meters below mean water, where mean water was 6.7 m below the concrete deck of the NUC tower.

All the readings were taken within 4 1/2 consecutive hours at night and early in the morning on October 22, 1971. The obtained data are given in Appendix A.

V. DATA REDUCTION

Five twenty-minute runs (split into ten two-minute individual records) make up the recorded analog data. The approach used was to read this information out on a strip-chart recorder, to digitize the printed analog data, and to use a computer to carry out a statistical and spectral analysis.

The phase fluctuation and the other oceanographic parameters were initially recorded at 1 7/8 inches per second. The tape recorded data were played back at 7 1/2 inches per second and first recorded on an eight channel Brush Mark 200 strip-chart recorder in order to allow visual comparison between the various sensor outputs (Fig. 4).

The tape recorded data was then played back a second time at 7 1/2 inches and recorded on a two channel Brush strip-chart recorder. This compressed the 20 minute run to five minutes and resulted in an increase in frequency by a factor of four. The strip-chart recorder was set at 25 mm/sec. chart speed and 10 mV/div sensitivity, corresponding to 1 degree/div.

The strip-chart records for each frequency at each depth were digitized using the Fleet Numerical Weather Central facility tracing digitizer at Point Pinos, California. The digitizer sampled the trace in increments of hundredths of an inch in the y-direction for each one one-hundredth of an inch advance in the x-direction and recorded this on a nine-track magnetic tape. Every record was digitized by first following the zero Volt reference line on the strip-chart and then moving the tracer vertically at the start of a record from the base-line onto the trace.

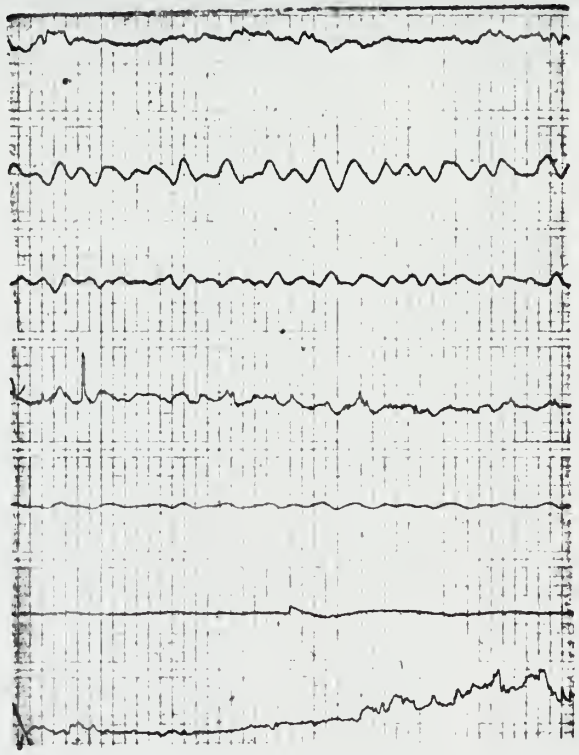

Fig. 4. Strip-Chart Record of Oceanic and Acoustic Data

By doing this it was assured that the digitized data points were absolute values referenced to zero Volt. Thus, the scaling factor in the y-direction is

$$.254 \text{ mm/data point} \triangleq .254 \text{ degree/data point}$$

resulting in

$$.254 \text{ mm/d.p.} \times \frac{1}{25} \text{ sec/mm} = .01016 \text{ brush sec/d.p.}$$

$$= .04064 \text{ real sec./data point}$$

This implies that the sampling rate is 25 Hz and the Nyquist rate is then 12.5 Hz.

The digitized data were read out from the magnetic tape and punched on data cards using the Fleet Numerical Weather Central's CDC 5000 computer (see Computer Program 1). The data cards could then be used for analysis on the USNPGS IBM 360 digital computer.

VI. COMPUTATIONAL METHOD

Since we were working with a continuous wave method the signal received by the first hydrophone can be written as

$$y_A = a \sin(\omega t)$$

and the signal received by the second hydrophone B has then to be written

$$y_B = b \sin(\omega t - kx)$$

where k = the wave number $= \frac{\omega}{c} = \frac{2\pi f}{c}$

f = the frequency of the applied signal

c = the phase wave velocity

x = the separation between the hydrophones

Since we compare the two signals with respect to phase by using the digital phase meter we have to find values for ω for which

$$kx = \psi$$

where ψ is the total phase difference between the two signals due to an integral number of wave lengths and a fraction of the wave length. We write

$$kx = (2\pi)n + \phi \qquad n = \text{an integer}$$

$$kx = \frac{\omega}{c} x = (2\pi)n + \phi$$

$$c = \frac{\omega x}{(2\pi)n + \phi}$$

$$c = \frac{fx}{n + \frac{\phi}{2\pi}} \qquad \text{where } \phi \text{ is in radians}$$

The final result will be

$$c = \frac{fx}{n + \frac{\phi}{360}} \qquad \text{where } \phi \text{ is in degrees}$$

Therefore the speed of sound may be obtained by using the measured frequency at which a phase difference ϕ was noted. In addition, x and n must be known. The integer n can be found by calculating c from the Wilson equation (Kinsler and Frey, Eq. 15.1) using readings for the temperature and the salinity. We find

$$\lambda = \frac{c}{f}$$

and then

$$n = \frac{x}{\lambda}$$

VII. BUBBLE THEORY

The speed of sound through a fluid is given by

$$c = \frac{\omega}{k}$$

where ω = sound frequency

$k = 2\pi/\lambda$ = propagation constant in bubble-free water

Following the analysis carried out by Morse and Feshbach, an incident acoustic pressure, of wave length very large compared to the bubble radius R, having a velocity potential $\psi_i e^{-i\omega t}$, will produce a total field averaged over all possible sizes and configurations of bubbles when written in differential equation formulation of

$$\nabla^2 \langle \psi \rangle + k_b^2(r) \langle \psi \rangle = 0$$

where

$$k_b(r) = k + \frac{2\pi}{k} \int_R \frac{n(r,R)\, R\, dR}{(\omega_o/\omega)^2 - 1 - i\delta(\omega_o/\omega)}$$

r = coordinate position of scattering region

k_b = propagation constant in bubbly water

R = bubble radius

ω_o = resonant frequency of bubble

δ = damping constant of bubble

$n(R)dR$ = number of bubbles per unit volume in radius increment R to R + dR

The quantity $\frac{k_b(r)}{k}$ is the index of refraction in the bubbly region and the real part defines the local speed of sound. This term is

$$\mathrm{Re}\{k_b(r)\} = k + \frac{2\pi}{k} \int_R \frac{R\, n(R)\, [(\omega_o/\omega)^2 - 1]\, dR}{[(\omega_o/\omega)^2 - 1]^2 + \delta^2(\omega_o/\omega)^2}$$

$$c = \frac{\omega}{k} = \frac{\omega}{k + \frac{2\pi}{k}\int_R \frac{R\, n(R)\, [(\omega_o/\omega)^2 - 1]\, dR}{[(\omega_o/\omega)^2 - 1]^2 + \delta^2(\omega_o/\omega)^2}}$$

$$\simeq \frac{1}{\frac{1}{c_o} + \frac{2\pi c_o}{\omega^2} \sum_i \frac{R_i\, n(R_i)[\omega_o/\omega)^2 - 1]\, dR_i}{[(\omega_o/\omega)^2 - 1]^2 + \delta^2(\omega_o/\omega)^2}}$$

where

$$n(R)\, dR = \frac{u(R)\, dR}{4/3\, \pi R^3}$$

$$n(R_i)dR_i = \frac{u(R_i)\, dR_i}{4/3\, \pi R_i^{\,3}}$$

$u(R)\, dR$ = fractional air to water volume for the increment between R and R + dR

$u(R_i)dR_i$ = fractional air to water volume for the increment between R_i and R_i + 1/n

Therefore we can write

$$c = \frac{1}{\frac{1}{c_o} + \frac{3c_o}{2\omega^2} \sum_i \frac{u(R_i)\, dR_i}{R_i^{\,2}} \frac{[(\omega_{o_i}/\omega)^2 - 1]}{[(\omega_{o_i}/\omega)^2 - 1]^2 + \delta_i^{\,2}(\omega_{o_i}/\omega)^2}}$$

This is the dispersion relation that predicts a decrease of sound speed caused by bubbles of resonance frequency greater than the incident frequency and an increase of sound speed for bubbles with lower resonant frequencies than the impinging sound.

The resonance frequency of clean air bubbles in water is given by (Eckart, 1945)

$$f_o = \omega_o/2\pi = (1/2\pi R_o)[(3\gamma P_o/\rho_o)(g/\alpha)]^{+1/2}$$

where γ = ratio of specific heats of bubble gas (=1.402 for air)

P_o = ambient pressure at bubble depth

ρ_o = density of surrounding water

The factor g is due to the influence of surface tension, it differs from unity only for very small bubbles, for the smallest bubbles of this study (R_o = 50 microns) g = 1.02. The factor α^{-1} modifies the value of γ, i.e., $\gamma\alpha^{-1}$ is the effective ratio of specific heats and lies for the smallest bubbles of this study in the range $1.24 < \gamma\alpha^{-1} \leq 1.40$. The two effects are to some extent mutually counteracting in their effect on the resonance frequency and therefore the term $\gamma g/\alpha$ will be assumed to equal 1.33.

The damping factor as a function of bubble resonance frequency as given by Devin will be approximated by

$$\delta_i = .027\,[\omega_{o_i}/2\pi \times 10^3]^{0.322}$$

VIII. EXPERIMENTAL RESULTS

Five different freqency sweeps have been carried out, runs 6 and 7 at a depth of 4.3 m and the remaining three, runs 8, 9, and 10, at 9.3, 14.3 and 7.3 m depth, respectively.

Run 6 covered a total frequency range from 25 - 80 kHz in steps of approximately two kHz. to be able to detect the detailed variations in the speed of sound; for the remaining runs readings were taken every four kHz. in order to examine the frequencies of interest in as short a period of time as possible. Run 7 started on hour after the end of run 5, but for the five runs reported here all the readings were taken within 4 1/2 consecutive hours between 0350 and 0820 on October 22, 1971.

Single temperature and salinity readings taken at each depth and a single bathythermograph record taken at 8 a.m. (Fig. 5) allow one to calculate the speed of sound for bubble-free water; the Wilson equation is used in the following form:

$$c = 1449 + 4.6t - 0.055t^2 + 0.0003t^3 + (1.39 - .012t)(S-35) + 0.017d$$

where c = speed of sound in meters per second

t = temperature in degrees centigrade

S = salinity in parts per thousand

d = depth in meters

The bubble-free values obtained for 4.3, 9.3 and 14.3 m are used as references for the dispersion curves and are included in Fig. 6.

The calculated values for the speed of sound based on the obtained data are examined and analyzed with respect to a frequency — and/or depth — dependence. If there is any change in c with frequency then this change

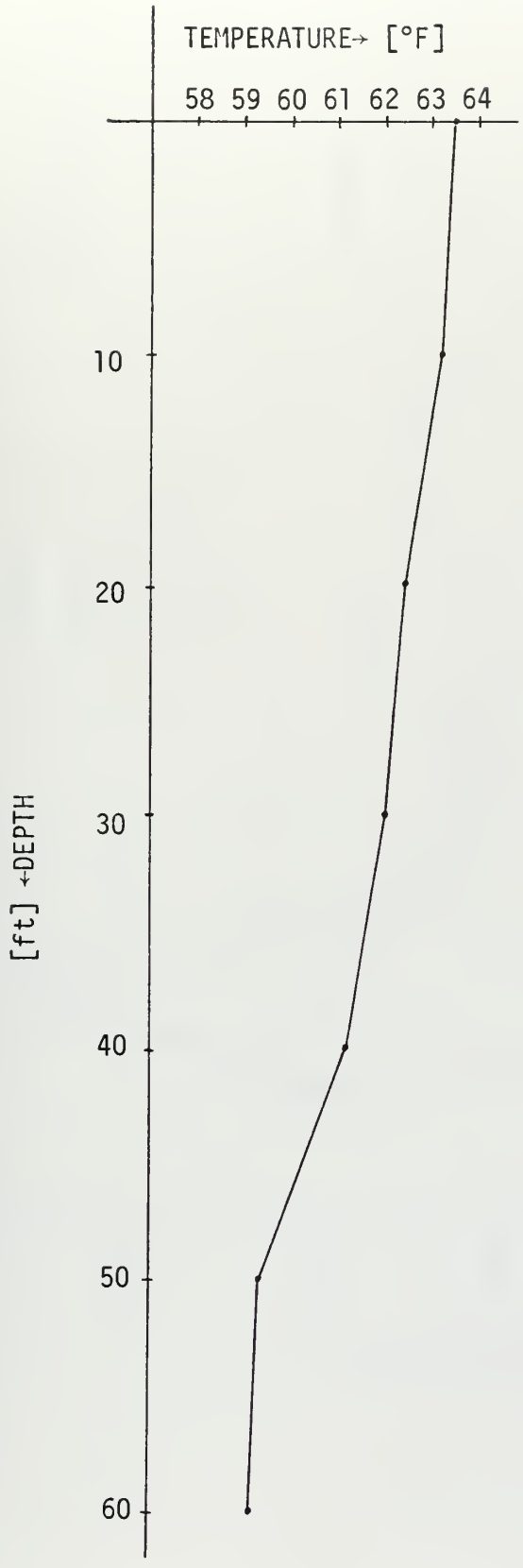

Fig. 5.

Bathythermograph Approximation
for 22 October 1971, 0800

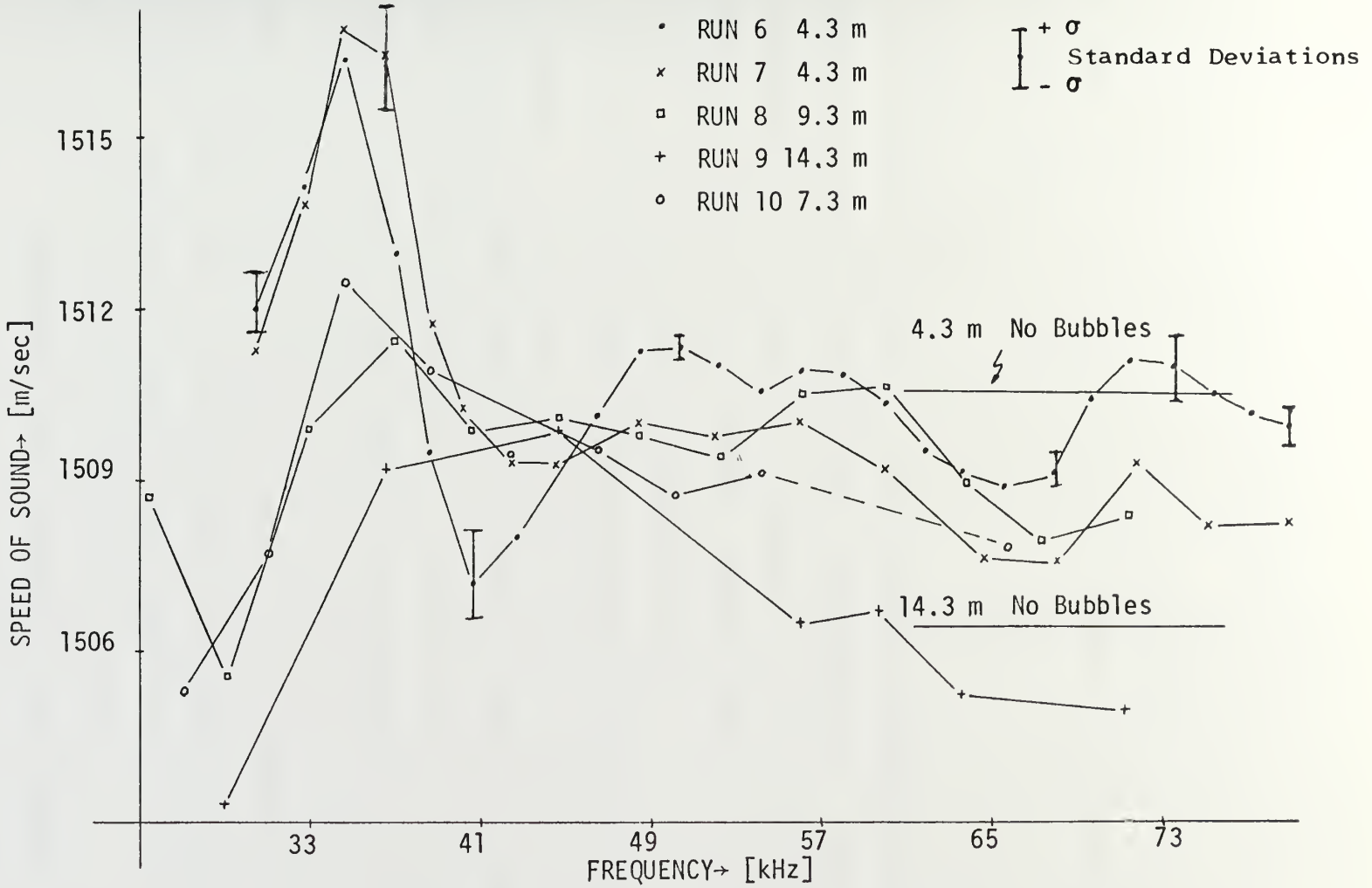

Fig. 6. Speed of Sound as a Function of Frequency and Depth

is attributed in general to either molecular relaxation or bubbles since for the sea-water medium no other frequency-dependent mechanisms are known at the frequencies of this study. But the magnitude of the molecular relaxation effect can be shown to be negligible (a frequency shift from 20 to 70 kHz. results in a $\Delta c \simeq 0.3$ m/sec.) as compared to the bubble effects.

A. FREQUENCY BEHAVIOUR

All the calculated values of c as a function of frequency for the different runs have been plotted on Fig. 6 for comparison. They should be interpreted by making use of the reference value for the non-bubbly medium which, because of the temperature change, shifts by as much as 4.2 m/sec. in going from 4.3 m to a depth of 14.3 m.

The first point of interest is the dispersive variation of c at a single depth. The first run (6) was carried out at a depth of 4.3 m and examined frequencies from 30.7 up to 79.2 kHz during a 40 minute period of time. Most significant is the strong increase in the speed of sound by as much as 6 m/sec. compared to the non-bubbly value for c of 1510.47 m/sec. and caused by the peak at 34.7 kHz followed by a smaller negative change of 3 m/sec at 40.6 kHz. For frequencies from 47 to 60 kHz the speed of sound shows nearly no dispersive behaviour. The higher frequencies are characterized by another peak in the c-curve roughly one fourth the strength of the peak at 34.7 kHz.

Run seven is interesting since it covered the same frequency range and the same depth as run six but for the major part now in steps of four kHz rather than 2 kHz. Since this allows a comparison between the two runs, a reminder is necessary that there is a time lag of one hour between the end of run six and the start of run seven. This time delay

may account for the slight shift in the dispersion curve downward and to the right. The shape matches the previous one pretty well, with two peaks clearly discernible.

In run eight the depth is increased by five meters as compared with the previous run. The main feature is a resonance pattern with a weaker maximum at 36.8 kHz rather than 34.7 kHz at shallower depth.

Run nine, at the greatest depth (14.3 m), differs in the pattern for the speed of sound over the frequency range by showing an increase in c over a wide frequency band with a maximum at approximately 41 kHz and no second peak. The obvious shift in the level is caused by a decrease of the non-dispersive value of c from 1510.47 at 4.3 m to 1506.27 m/sec at 14.3 m.

Run ten was made back at a depth of 7.3 m. The two readings at 57.7 and 61.59 kHz are believed to be non-representative since a boat approaching the tower injected a large number of bubbles into the volume under consideration. Excluding these data points, the dispersion curve shows a main peak around 35.5 kHz.

Summarizing the dispersion data it can be stated that:

1) The change of the speed of sound with frequency at sea was observed to be significantly stronger than expected.

2) The change in the speed of sound does not follow the usual dispersive pattern for a single dominant bubble regime.

3) The speed of sound curve at 4.3 m has two peaks. The frequency of the lower peak changes from 34.7 kHz at 4.3 m to 41 kHz at 14.3 m, which is a shift toward higher frequencies as expected for surface-generated bubbles carried downwards "isothermally" by turbulence. However, the shift is smaller than expected: isothermally convected identifiable,

non-diffusing, surface-initiated bubbles which resonate at 35 kHz at 4.3 m would resonate at 54 kHz and not at the observed 41 kHz when they reach 14.3 m. There are two explanations that can be proposed for this discrepancy:

a) the presence of the higher frequency peak in the near-surface measurement has shifted the low frequency peak to higher frequencies than it would have had by itself. The absence of the second peak in the deeper measurement (due to more rapid disappearance of smaller bubbles) permits the low frequency peak to more accurately identify the resonance frequency of these bubbles. We herein assume that near the surface we encountered a bubble population made up of larger surface-generated bubbles and smaller bubbles introduced primarily by continental aerosols that drop into the water. To check on the dispersion curve that results from a specific bubble distribution, a bubble population was created peaking around 60 and 120 microns as given in Fig. 7. Subsequently the computer program (3) was written calculating the speed of sound dispersion based on the equations derived in Section VII and using the above mentioned volume concentration of bubbles. The result is a dispersion curve given in Fig. 8 which is in good agreement with our data obtained at 4.3 m. The observed dispersion curves for the other depths support this hypothesis, since only part of the larger bubbles are carried down, decreasing in number with increasing depth whereas the smaller bubbles rapidly disappear due to gas diffusion out of the bubbles.

b) the larger bubbles originate in the volume or at the bottom, rather than at the surface. As they rise they lose gas by diffusion, so that when they reach the surface they are not as large as predicted by the non-diffusion assumption and are thereby at higher frequencies than expected.

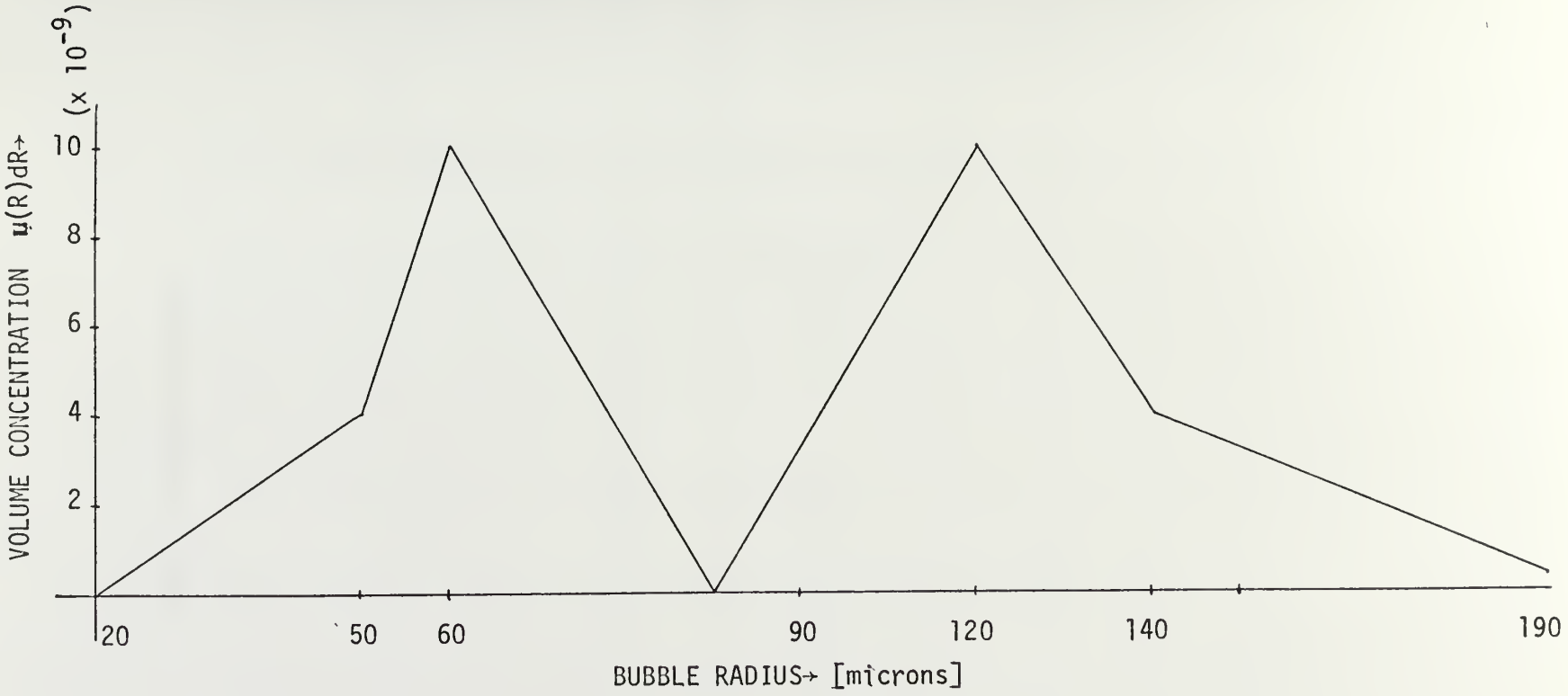

Fig. 7. Postulated Volume Concentration versus Bubble Radius

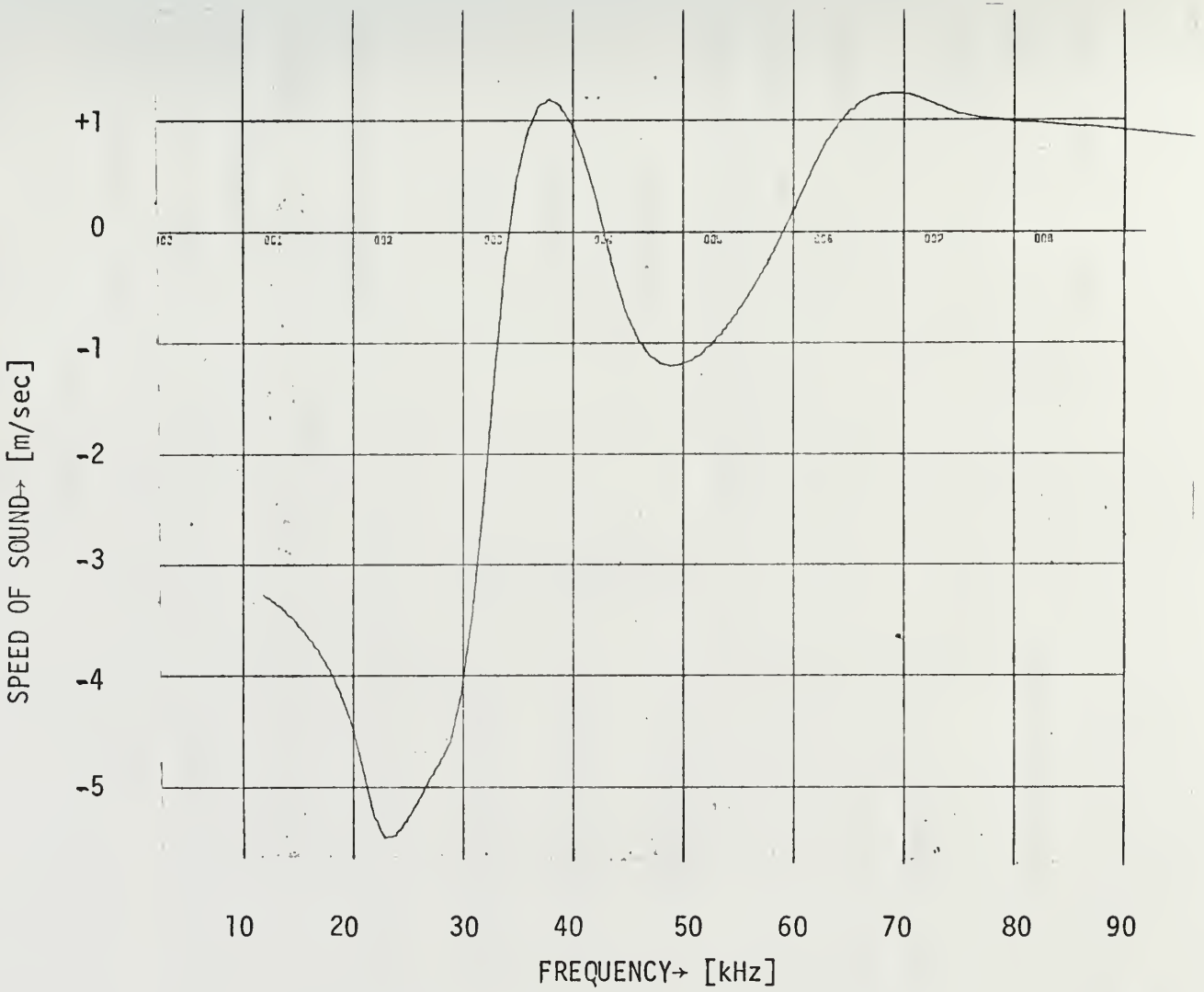

Fig. 8. Speed of Sound Dispersion for Bubble Population of Fig. 7

B. DEPTH BEHAVIOUR

Next the variation in c with depth for a constant frequency will be considered. On the assumption that the bubble densities were not a function of time during the 2 1/2 hours of runs 7-10, all these data have been rearranged to display the variation in the speed of sound with depth at various constant frequencies as given in Table I. These values have been used to plot the speed of sound versus depth in Fig. 9. These straight line segments reflect the major variations in c with frequency as described in the last section.

In order to examine the variation of the speed of sound versus depth, it is necessary to subtract out first all possible temperature, salinity, and pressure-based changes with depth. To do this, use is made of the following coefficients for variation with

temperature	$\frac{\Delta c}{\Delta T} = + 5$ ft/(sec) (°F)
salinity	$\frac{\Delta c}{\Delta S} = + 4$ ft/(sec) (ppt)
depth	$\frac{\Delta c}{\Delta z} = + 0.017$ ft/(sec) (ft)

The salinity changed by -.1 ppt over 10 m and therefore accounts for a change of c with S of -.4 meter per second. It is necessary to add to this a change of +.17 m/sec due to the depth effect such that the total effect of salinity and depth on c will be -.23 m/sec when going from 4.3 to 14.3 m; this small effect will be neglected.

The temperature-caused changes in the speed of sound have to be taken into consideration. The BT curve sketched in Fig. 5 is approximated by straight line elements and is used with the Wilson equation to calculate values for the speed of sound at different depths for the

TABLE I. Speed of Sound in m/sec

Depth (m) / Freq. (kHz)	4.3	4.3	7.3	9.3	14.3
28.97				1505.73	1503.28
30.70	1511.99	1511.37	1507.67		
32.77	1514.18	1513.88		1509.89	
34.76	1516.46	1516.94	1512.51		
36.79	1512.90	1516.52		1511.55	1509.2
38.73	1509.48	1511.82	1510.93		
40.61	1507.30	1510.22		1509.89	
42.50	1508.13	1509.30	1509.53		
44.47		1509.39		1510.17	1509.89
46.40	1510.29		1509.62		
48.36	1511.31	1510.05		1509.84	
50.27	1511.36		1508.78		
52.20	1511.03	1509.79		1509.36	
54.12	1510.74		1509.20		
56.03	1510.92	1509.99		1510.66	1506.56
59.88	1510.31	1509.19		1510.64	1506.78
63.67	1509.11	1507.65		1508.95	1505.43
65.62	1508.11		1507.86		
67.54	1509.14	1507.55		1507.92	
71.42	1501.32	1509.26		1508.42	1505.01

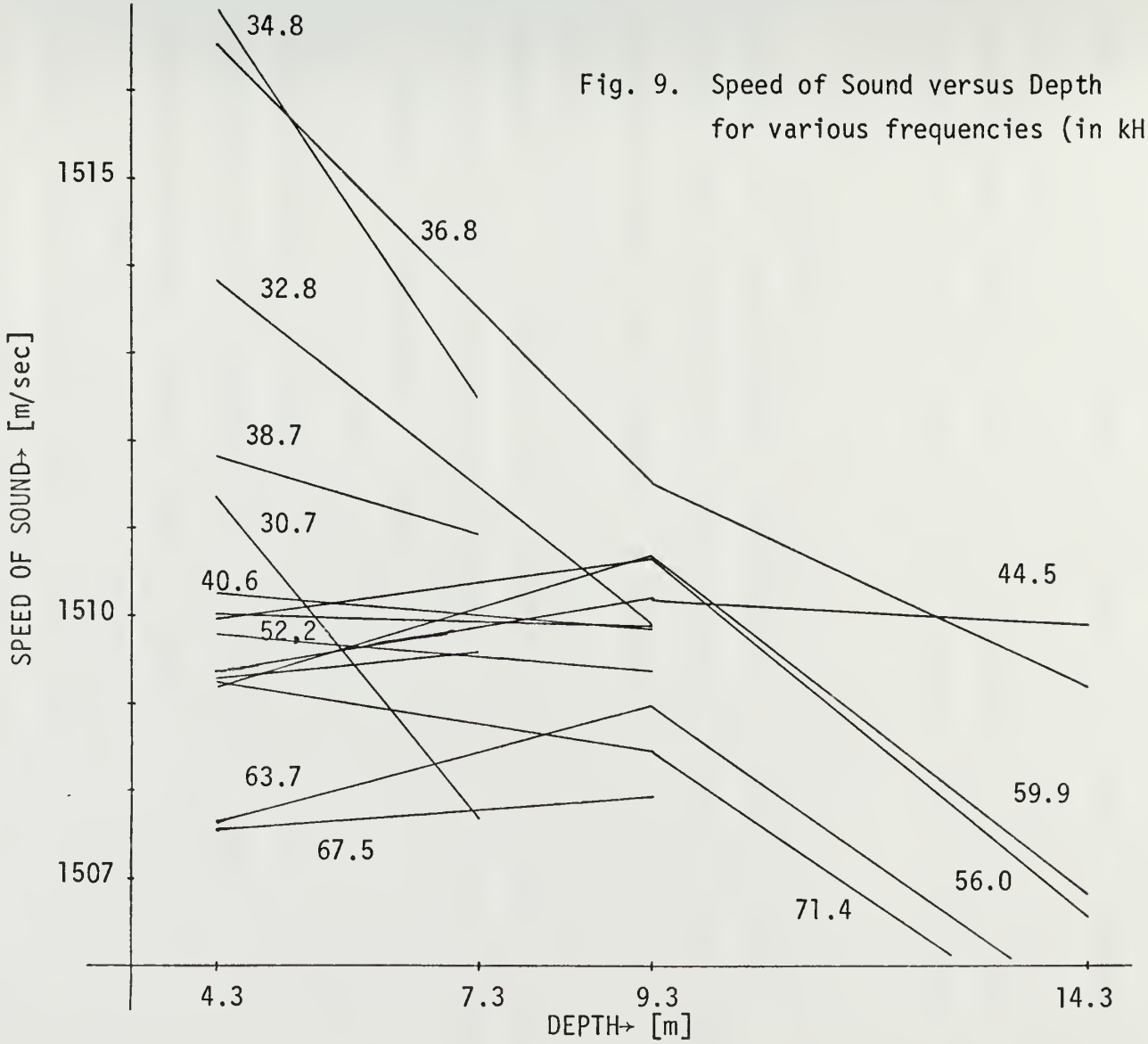

Fig. 9. Speed of Sound versus Depth for various frequencies (in kHz)

the non-bubble case. After doing this it is possible to compare the measured values of c with the values for bubble free sea water. The plot of the temperature-caused changes has to be referenced to a value of c that holds for the bubble-free medium and the previous calculated value of 1506.27 m/sec at 14.3 m was used. The non-bubble theoretical value of c is subtracted from the measured value and the difference is then called Δc_B, due to bubbles, which is plotted on the same graph. Since the shift in the frequency peaks causes the pattern of the measured c versus depth plot to be markedly different for the various frequencies, five different frequencies have been picked that are felt to be representative for the total frequency region: 36.79, 44.47, 56.03, 63.67, 71.42 kHz.

This representation of c versus depth at a constant frequency can only be used to examine whether one encounters, at a specific depth, resonant bubbles such that for sound frequencies smaller than the bubble resonance frequency one experiences a decrease of sound speed and for impinging sound of higher frequencies than the resonance frequency an increase in c. It should be clear that this plot ignores depth effects on an identifiable surface-generated bubble carried to different depths.

Figure 10 presents this information for a frequency of 36.79 kHz. Since there is a strong positive Δc_B of 5.25 m/sec at 4.3 m this means that we encounter strong populations of bubbles with lower resonance frequencies than the impinging sound, in other words, there are many bubbles that resonate below 36.79 kHz. Figure 11 represents the situation at 44.47 kHz and shows that we sense bubbles of resonance frequency greater than the incident frequency at 4.3 m depth and of resonance frequency smaller than the incident frequency at 14.3 m. The picture

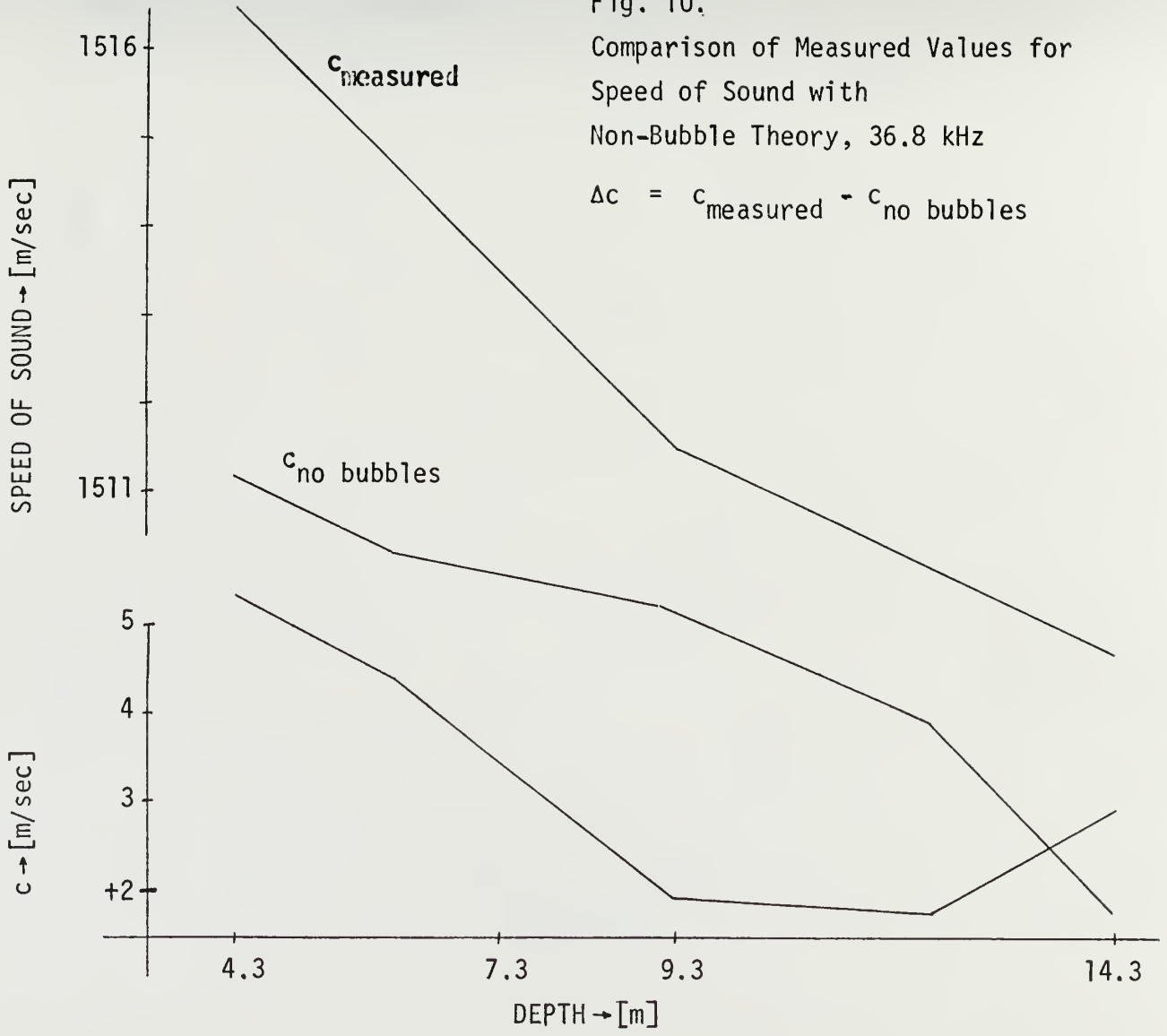

Fig. 10.
Comparison of Measured Values for Speed of Sound with Non-Bubble Theory, 36.8 kHz

$\Delta c = c_{measured} - c_{no\ bubbles}$

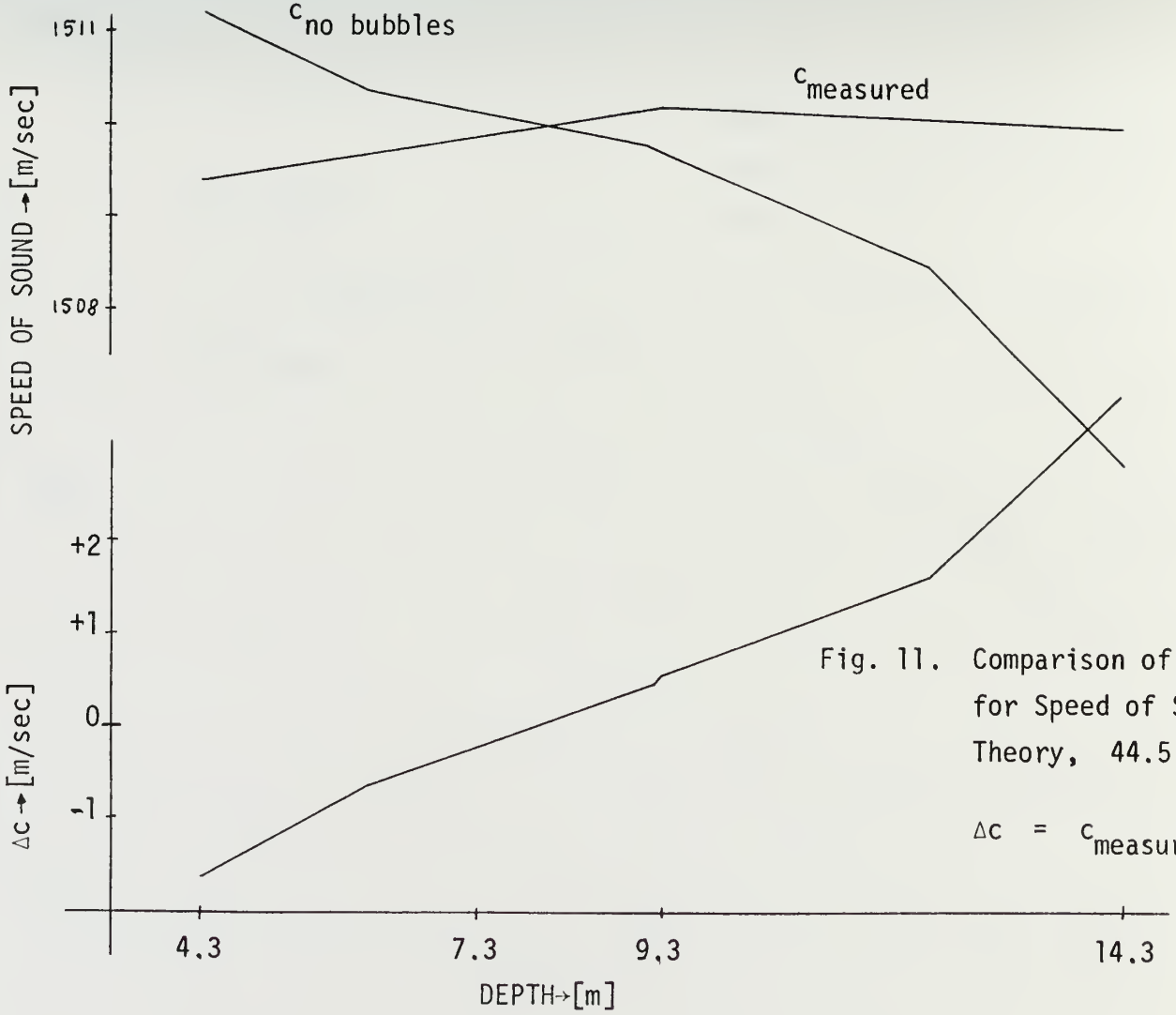

Fig. 11. Comparison of Measured Values for Speed of Sound with Non-Bubble Theory, 44.5 kHz

$\Delta c = c_{measured} - c_{no\ bubbles}$

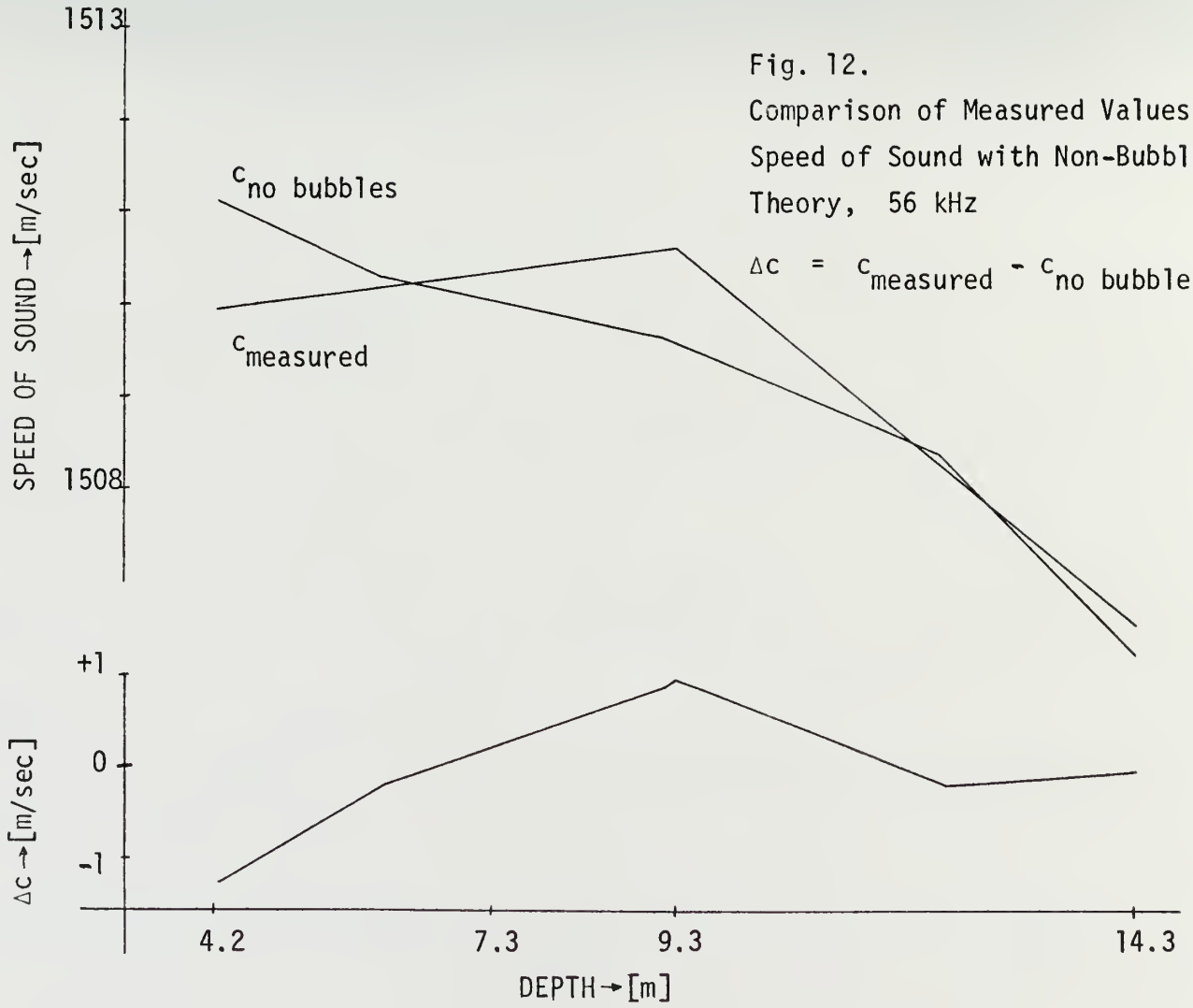

Fig. 12.
Comparison of Measured Values for Speed of Sound with Non-Bubble Theory, 56 kHz

$\Delta c = c_{measured} - c_{no\ bubbles}$

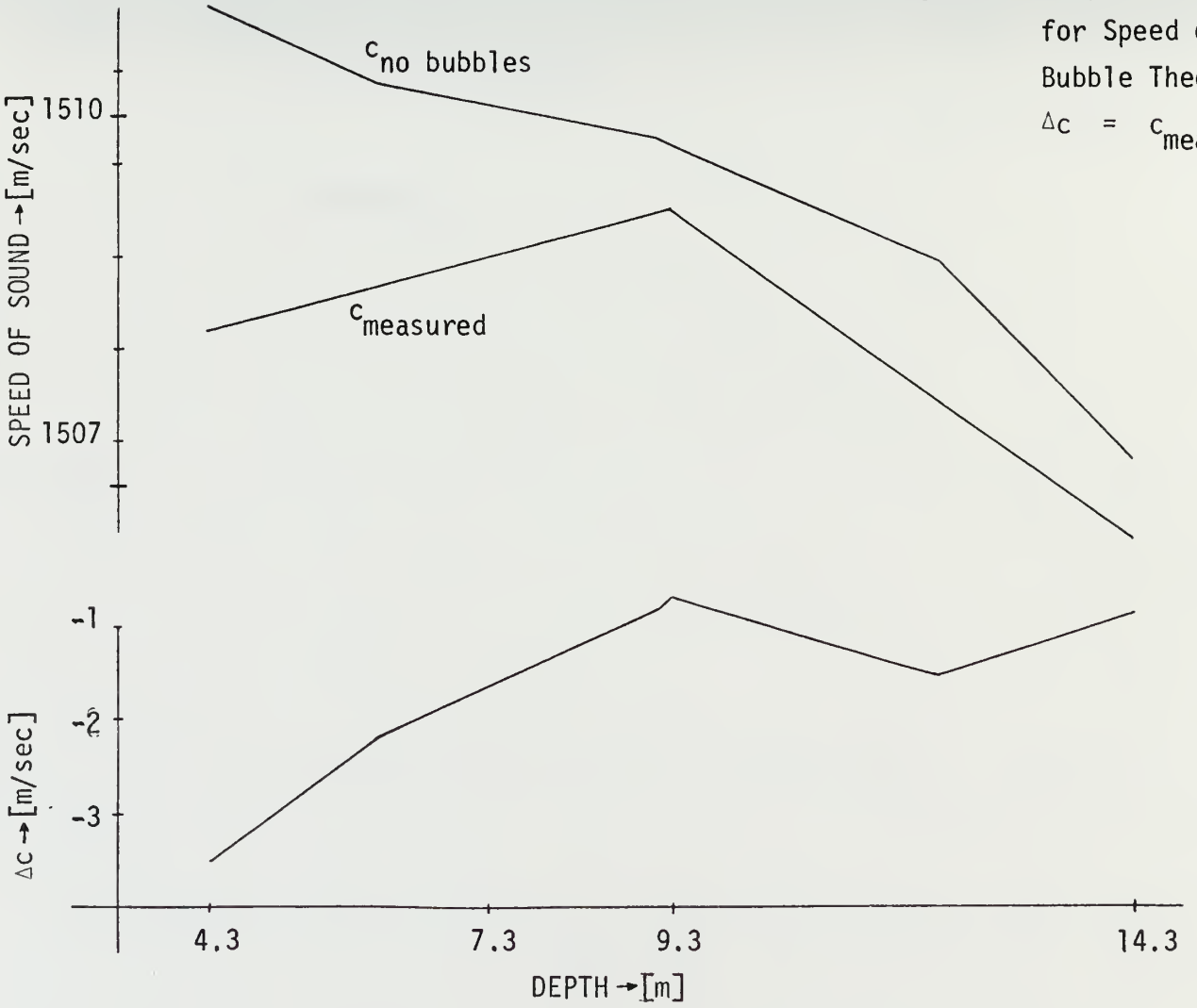

Fig. 13. Comparison of Measured Values for Speed of Sound with Non-Bubble Theory, 63.7 kHz

$\Delta c = c_{measured} - c_{no\ bubbles}$

Fig. 14. Comparison of Measured Values for Speed of Sound with Non-Bubble Theory

$\Delta c = c_{measured} - c_{no\ bubbles}$

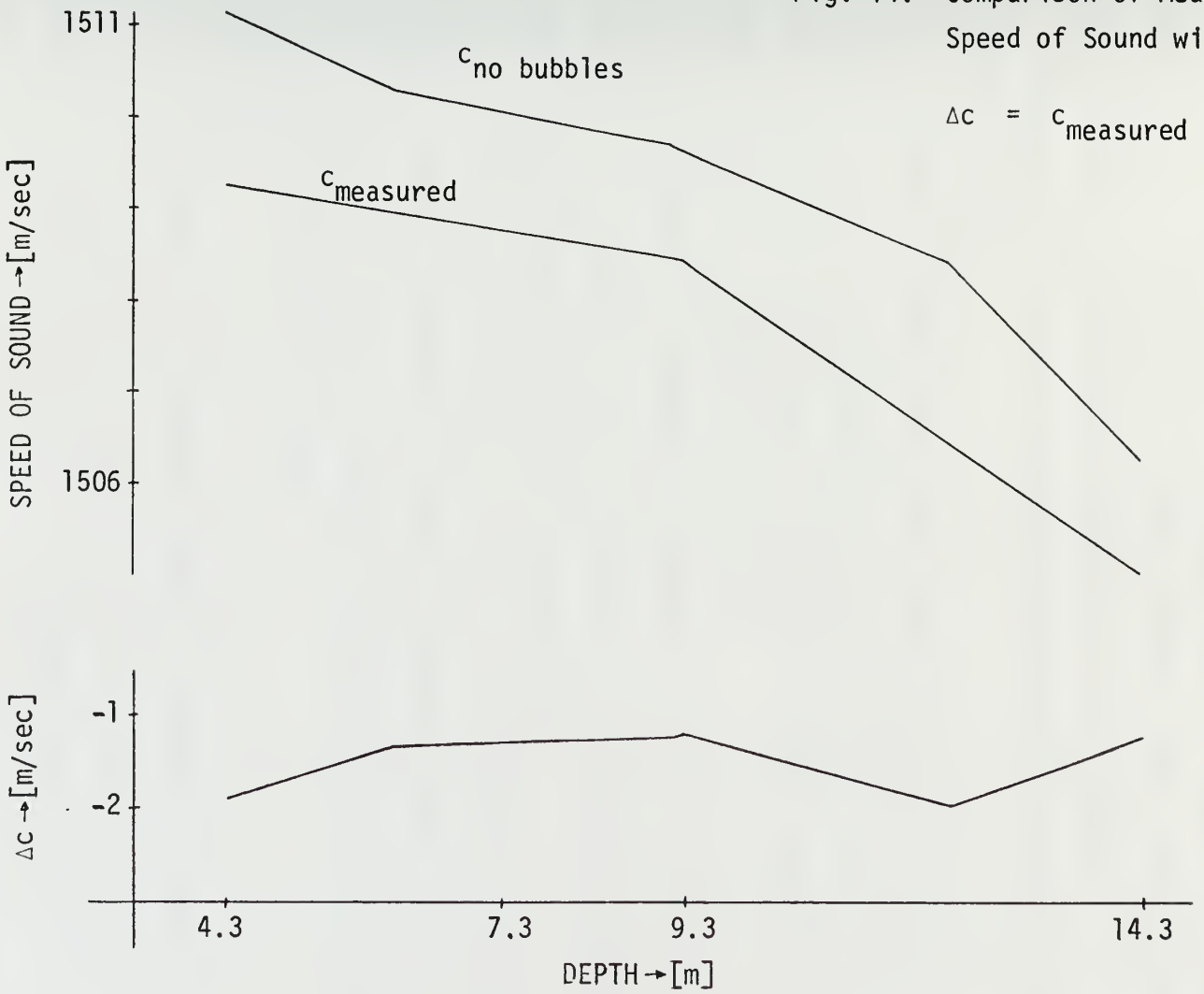

changes when going to Fig. 12. At a frequency of 56.03 kHz there is no significant dispersive behaviour at all. For frequency 63.67 kHz, Fig. 13, at all depths we sense bubbles of resonance frequencies greater than the frequency of the acoustical signal. Since the difference between the measured value and the non-bubble theoretical value is much larger at 4.3 than at 14.3 m we are either very close in frequency to resonant bubbles at 4.3 m or the population is considerably stronger than at 14.3 m. Figure 14, 71.43 kHz, finally shows a smaller negative Δc_B with only minor differences between the various depths.

Summarizing, we can make the following statements related to the different depths:

4.3 m: There is a large population of bubbles having a resonance frequency close to and somewhat smaller than 36.79 kHz. At 44.47 and at 56.03 kHz we sense and at 63.67 kHz we detect another population of bubbles with an ω_r greater than 63.67 kHz.

7.3 m: Bubbles with a resonance frequency less than 36.79 kHz are also detected at this depth. At 44.47 kHz we are far enough away from this region and encounter no dispersive characteristic.

9.3 m: There is a population of bubbles resonating below 36.79 kHz.

14.3 m: There are bubbles of resonance frequencies below 44.47 kHz. At 56.03 kHz this region of resonance frequencies has been passed and no dispersive behaviour is shown.

Conclusions:

At 4.3, 7.3, and 9.3 m we observed bubbles of resonance frequency below 36.79 kHz and above 71.42 kHz and at 14.3 m we found a broad region of bubbles resonating below 44.47 kHz. The sound speed dispersion is strongest at 4.3 m and is reduced in amplitude when going to a greater

depth. The conclusions derived from the variation in the speed of sound with depth are consistent with the observations made for the variation in the speed of sound with frequency.

IX. STATISTICAL AND SPECTRAL ANALYSIS

The signal received at hydrophone one does not have a constant phase difference with respect to that at hydrophone two but is a random signal. This is the equivalent of a noisy signal where the noise in this case is due to the integrated effects of time-varying speed of sound due to varying temperature, salinity and bubble patches along the sound path. It is assumed that the random signal exhibits statistical stationarity which is partially described in terms of a probability density function (P.D.F.) and the statistical moments. In addition to a statistical description it is valuable to use the time series to determine the temporal correlation function and the power spectral densities of the time-varying phase (Ref. 2).

The variable phase signal that we received at a specific frequency and for a period of approximately 90 sec is a continuously changing random variable within some finite interval. But since this recorded information is digitized, the random variable can assume only a finite number of distinct values so that we must treat it as a discrete random variable. In practice the recording technique used resulted in magnitude increments of .254° spaced in time by .04064 sec. For one frequency record we then get n data points. If A is one of the possible data points, then n_A is the number of times A occurred and the ratio n_A/n is the relative frequency of occurrence of the event A for that particular record. This approach allowed the use of the sampled data points to form a histogram that can be interpreted as a distribution function:

$$F(x) = P(\phi \leq x)$$

from which a density function can be obtained:

$$p(x) = \sum_i P(x_i)\, \delta(x - x_i)$$

Examining these histograms it turns out that the main pattern of the envelope follows a Gaussian distribution. This can be expected since in the experimental measurement many irregular and fluctuating causes like weak temperature and salinity inhomogeneities caused the phase reading to have small random variations which produce the Gaussian P.D.F. about the undisturbed value. It seems that the bell-shaped curve experiences stronger changes around 35 and 65 kHz. This different behaviour is pointed out by a series of historgrams (Figs. 15-19) for the latter frequency range and for 4.3 m depth. At 59.9 kHz the general shape is narrow Gaussian but at 63.7 kHz the distribution is nearly evenly spread over a wider center range that sharply drops at the skirts. At 67.6 kHz the envelope changes again and achieves at 69.6 kHz a wide Gaussian pattern. At 77.3 kHz the pattern is again that of a narrow Gaussian noise. Since this change in the density function is a particular phenomenon for frequencies around 35 and 65 kHz and is not found for frequencies in between, it is postulated that time varying resonant bubble populations predominantly around frequencies 35 and 65 kHz caused the variation with frequency. These frequencies are essentially the same as observed previously in the peaks in the analysis of speed as a function of frequency.

The statistical average, or mean value, $\bar{x}$ of the random variable ϕ has been used to calculate the mean speed of sound which is the expected value for c. By calculating the variance

$$\sigma_x^2 = \overline{(x - \bar{x})^2} = \overline{x^2} - \bar{x}^2$$

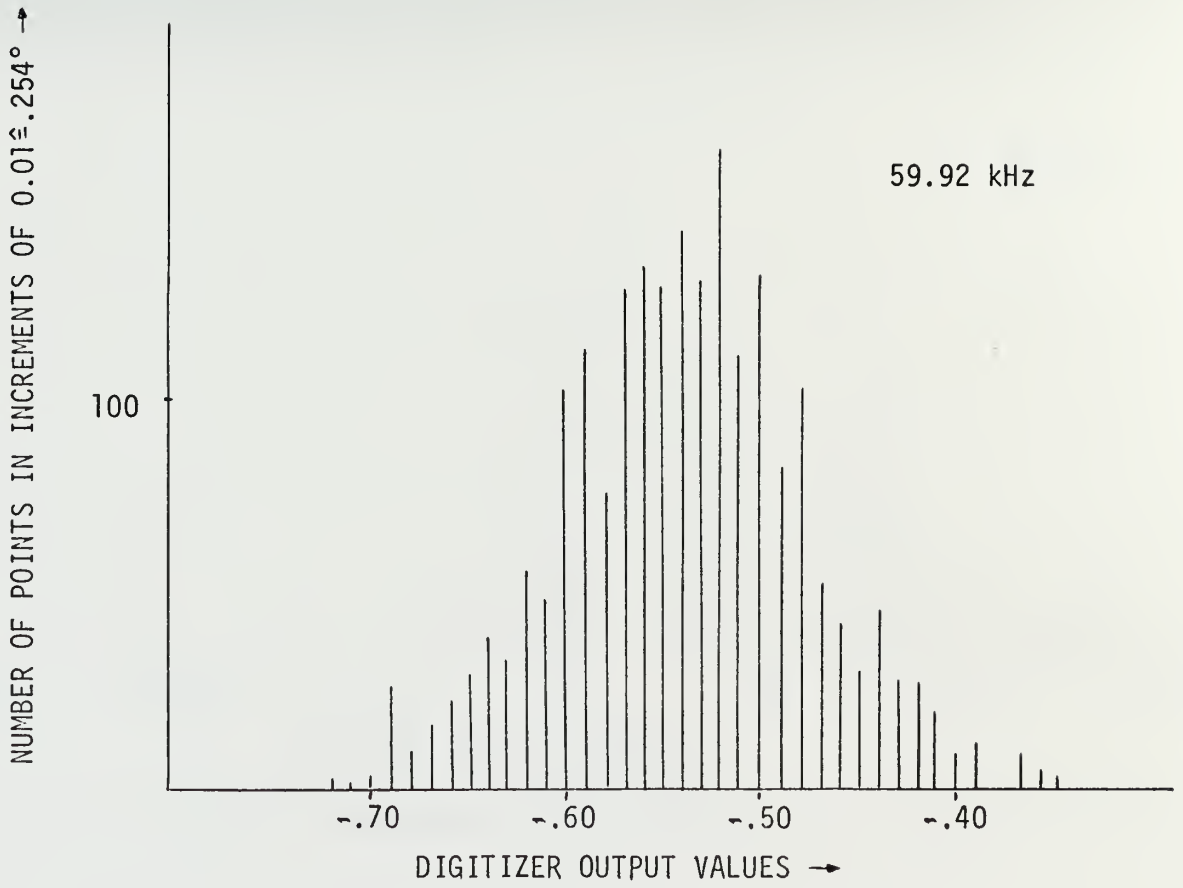

Fig. 15. Histogram of Phase Angle

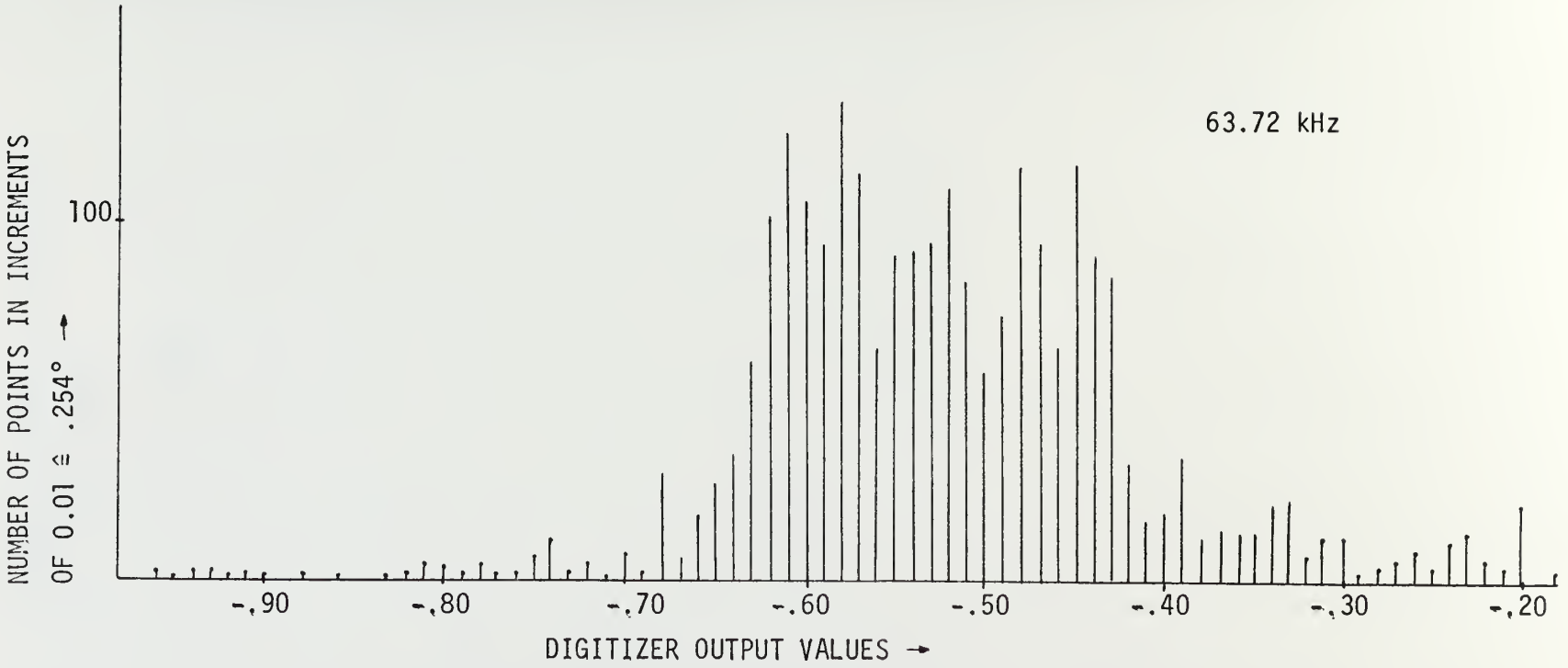

Fig. 16. Histogram of Phase Angle

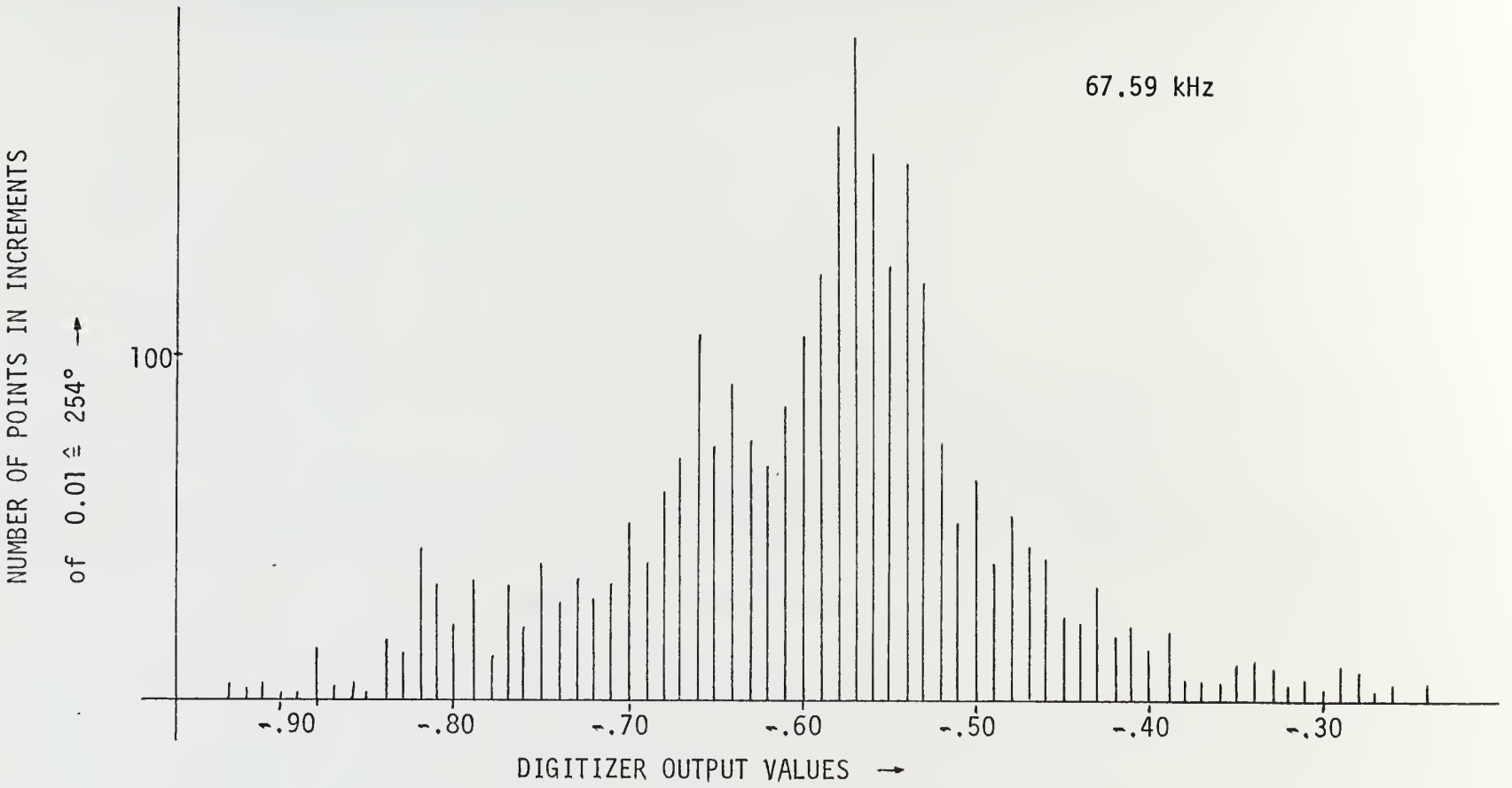

Fig. 17. Histogram of Phase Angle

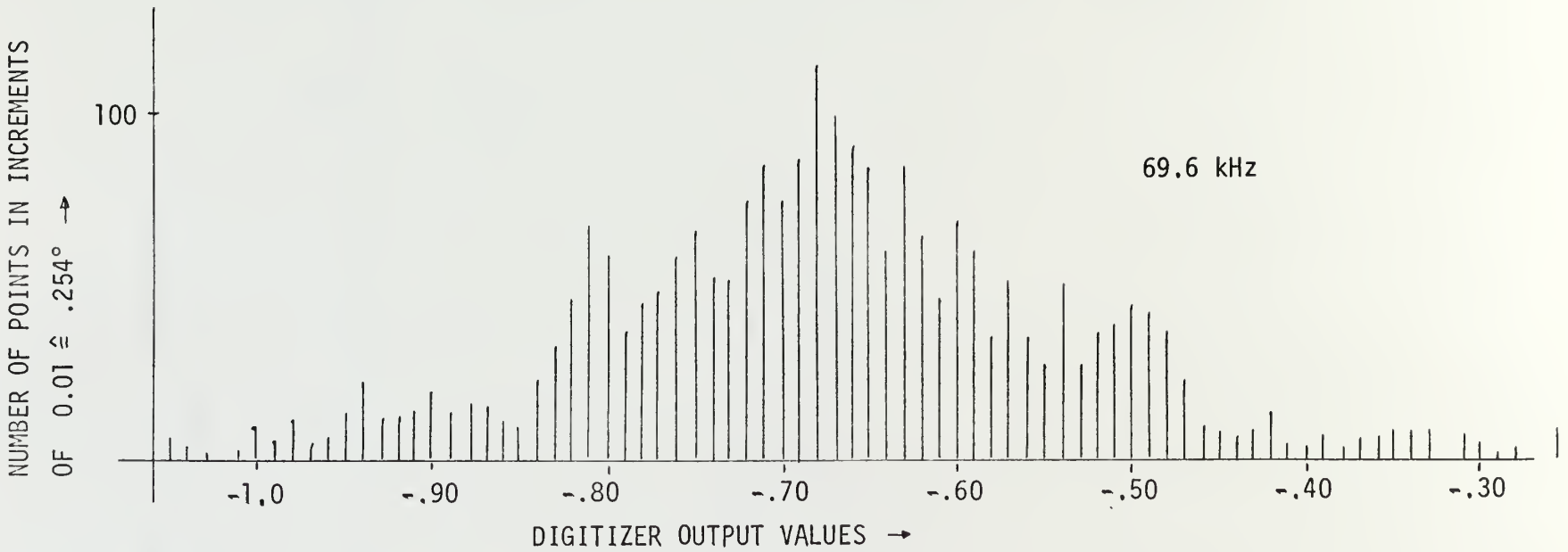

Fig. 18. Histogram of Phase Angle

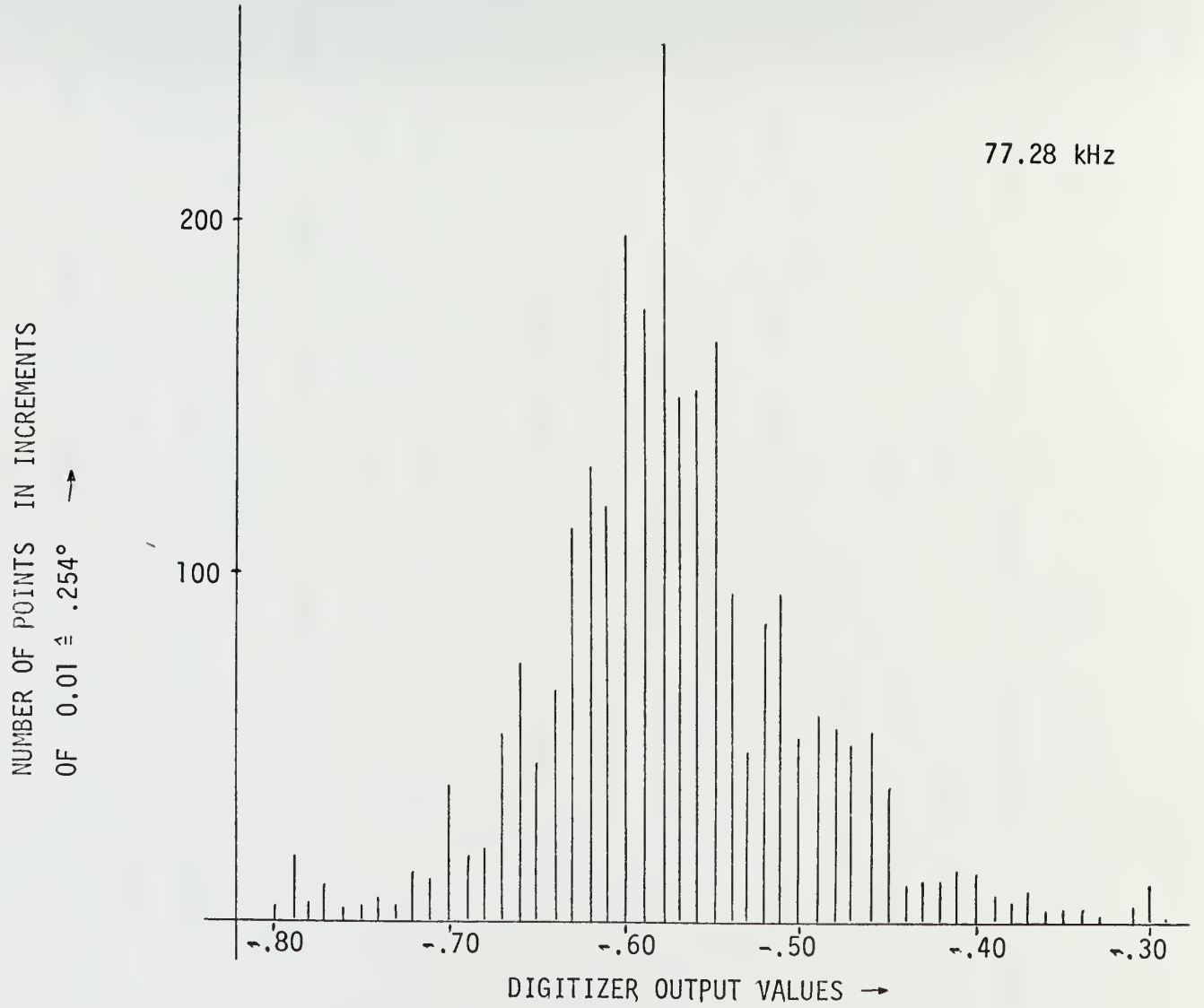

Fig. 19. Histogram of Phase Angle

and taking the square root of the variance to obtain the standard deviation, σ_x , one has a measure of the spread of the observed values. A large standard deviation implies a large spread of likely values for any given observation, and vice versa. The standard deviation was calculated for all frequency readings from 30.7 to 79.2 kHz and is plotted as a function of frequency in Fig. 20.

Since there was a time lag of two minutes between frequency runs, σ_x is for this case not only a function of frequency but also of time, which is increasing with frequency. To be able to judge which fraction of the variation in σ_x is a time effect and which is the frequency effect a continuous 20 min record of phase modulation at 60 kHz was split into ten two-minute records so that the standard deviation could be examined as a function of time alone (Fig. 21). Comparing the two graphs there is a mean value of 1.28° and a total variation of $\pm$ .32° for the time record; there is a much stronger excursion for the frequency plot which shows a mean value of 1.92° at 60 kHz with a deviation of + 1.92° at 40.6 and of + 2.56° at 69.6 kHz. One can rule out temperature and salinity patches as the causing agency for the effect in Fig. 20 since those would not show a frequency dependent spread of the measured values. It seems that the presence of bubbles in the medium causes this strong change in the standard deviation as a function of frequency. The frequencies of the peak values of σ_x are approximately the same as the frequencies already identified as centers of resonant bubbles.

Next the autocorrelation function $R(\tau)$ will be considered since it provides information about $\phi(t)$ and also relates to the frequency-domain description of the random signal. $R(\tau)$ is defined by

$$R(\tau) = \langle x(t)x(t+\tau)\rangle / \langle x(t)x(t+\tau)\rangle_{\tau=0}$$

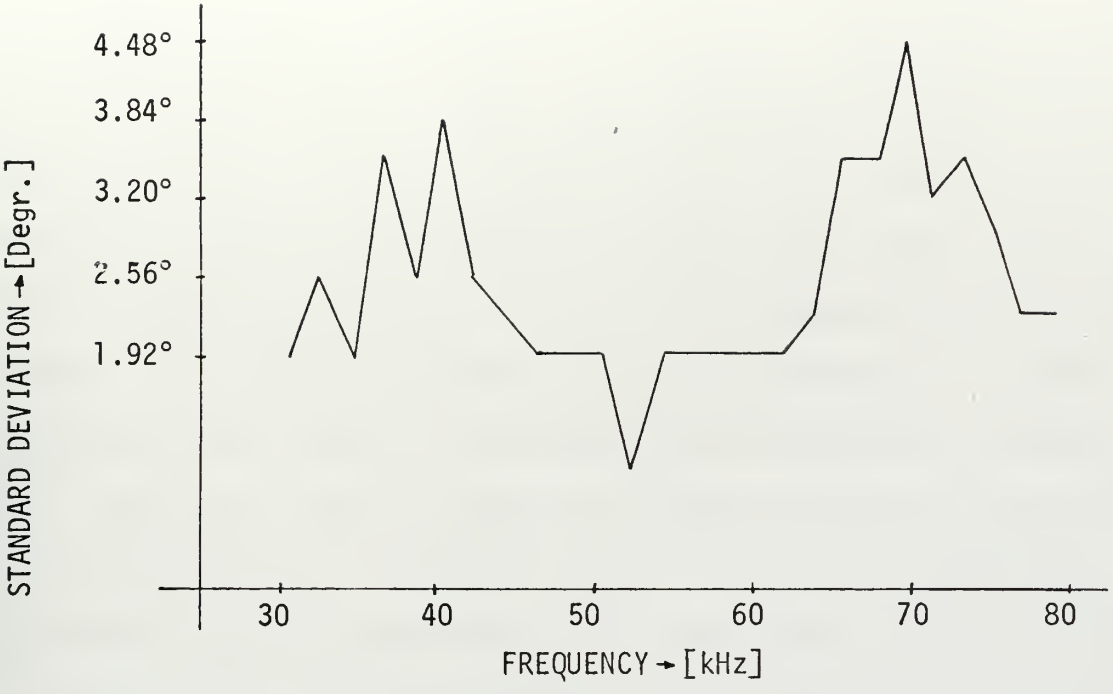

Fig. 20. Standard Deviation as a Function of Frequency. Time increasing with frequency

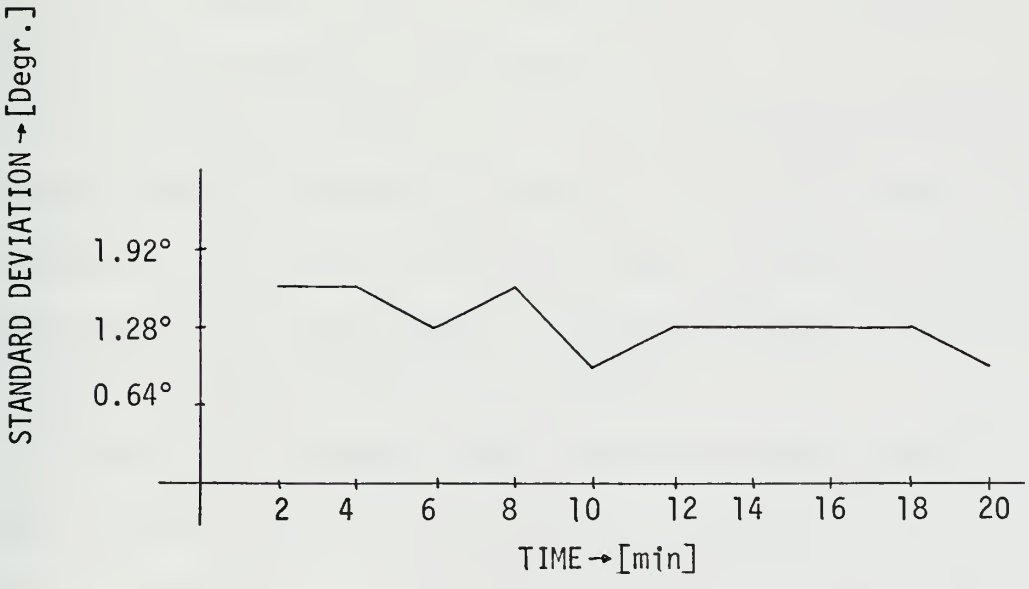

Fig. 21. Standard Deviation as a Function of Time Only at Frequency 60 kHz

It should be noted that the autocorrelation function is a measure of both temporal variation and statistical dependence. The plots of the normalized autocorrelation at 30.7 and 46.4 kHz are considered to be representative and are given in Figs. 22 and 23. The graph for 30.7 kHz shows a variation superimposed on the almost ideal damped cosine pattern obtained at 46.4 kHz. This variation is probably due to bubble effects. Recall that the frequency 30.7 kHz was observed as a predominant resonance frequency in the speed of sound discussion of section VIII. The time it takes for the autocorrelation to drop to 1/e of its value is plotted versus frequency on Fig. 24. No specific regularity can be found. On the average this "correlation time" is approx. 1.8 sec.

Examining the autocorrelation function we arrive at the following results: The phase modulation remains correlated (1/e) for 1.46 sec, the salinity for 3.96 sec and the speed of sound as measured by the velocimeter for 2.28 sec (Figs. 25-27). The temperature records have not yet been analyzed (thesis of LCDR Duchock to be issued March 1972). Since for the velocimeter (operating at 3 MHz) $c = c(T, S)$ it appears that the temporal variation in c is due principally to salinity patches (and most probably temperature patches). On the other hand, our phase measurement is a function of not only S and T but also of the bubble distribution. The still smaller correlation time of 1.46 sec is evidence of additional decorrelation due to bubbles.

Turning to the frequency domain, the power spectral density of the phase variation gives the distribution of average power of the fluctuations in frequency. To find the PSD the Mean Lag Product Method by Blackman/Tukey was used. The main feature of this method is to calculate not only the autocovariance function but in addition an apparent

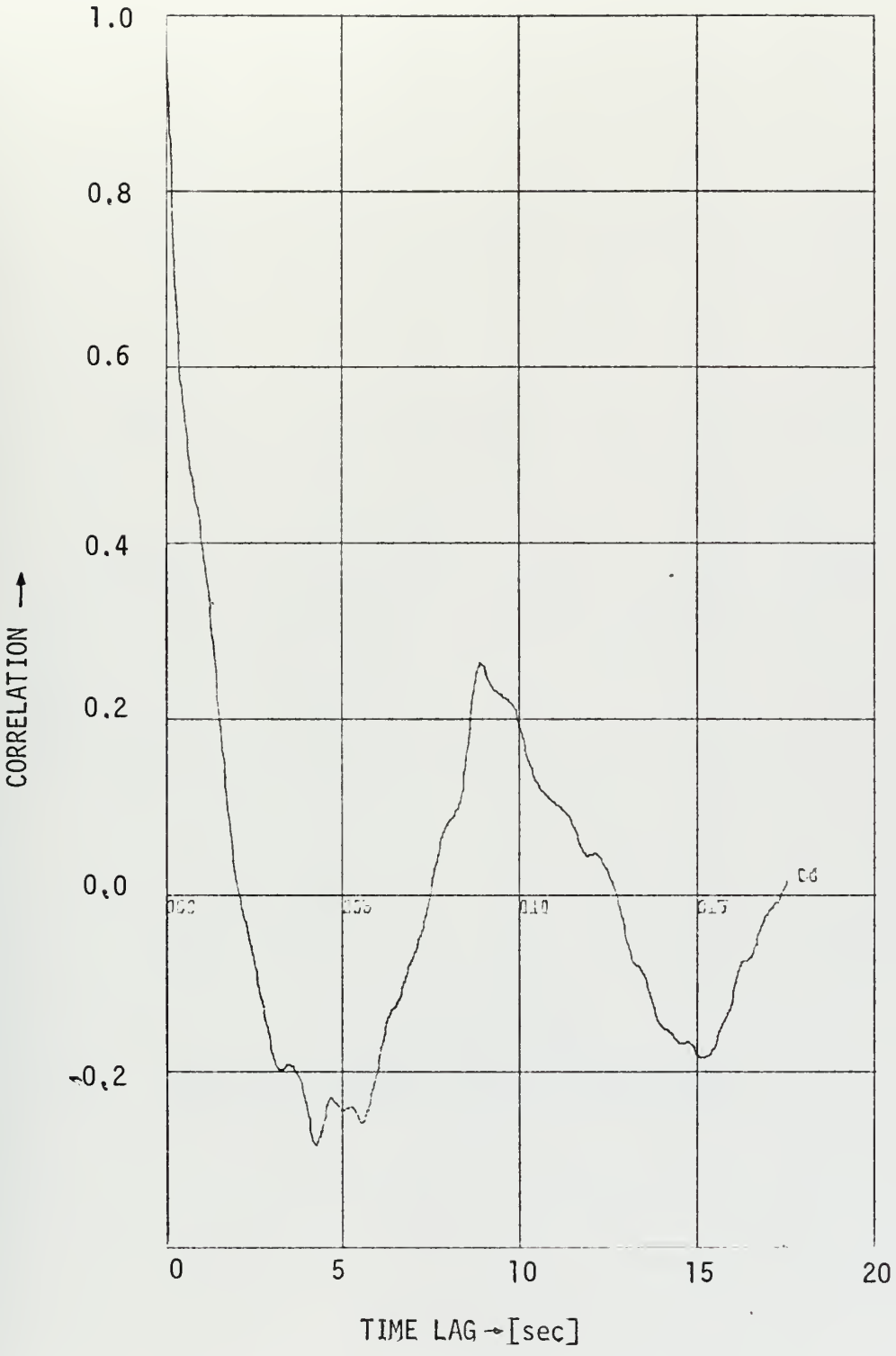

Fig. 22. Autocorrelation at 30.7 kHz

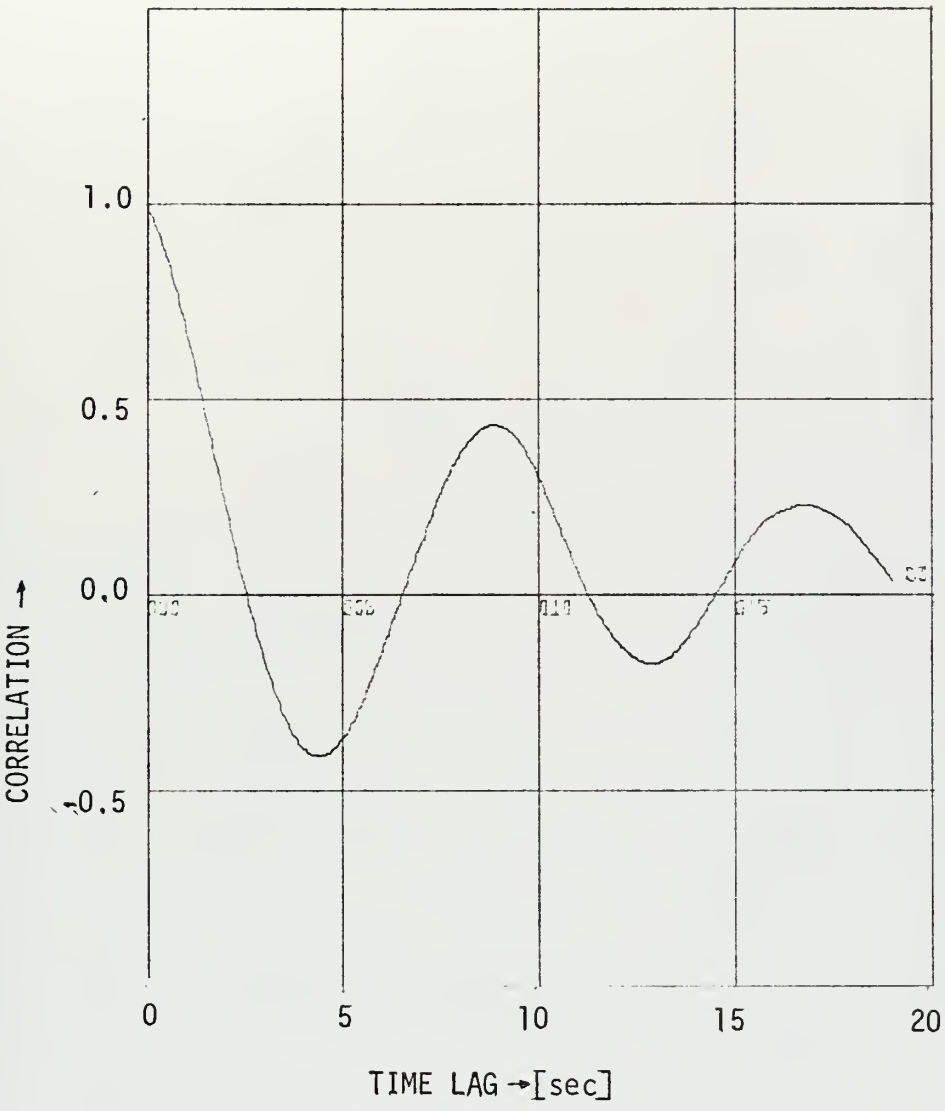

Fig. 23. Autocorrelation at 46.4 kHz

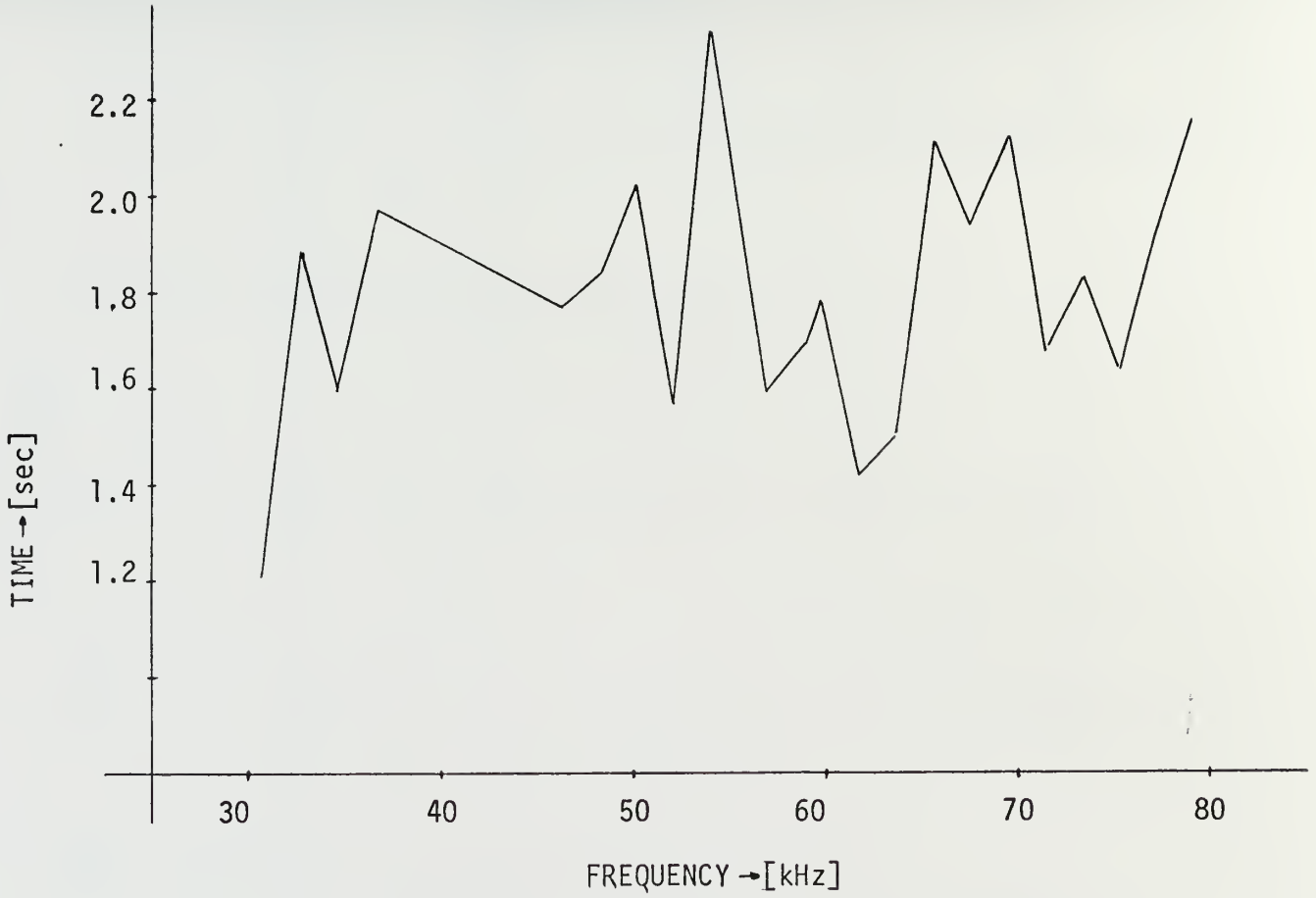

Fig. 24. Decorrelation Time as a Function of Frequency

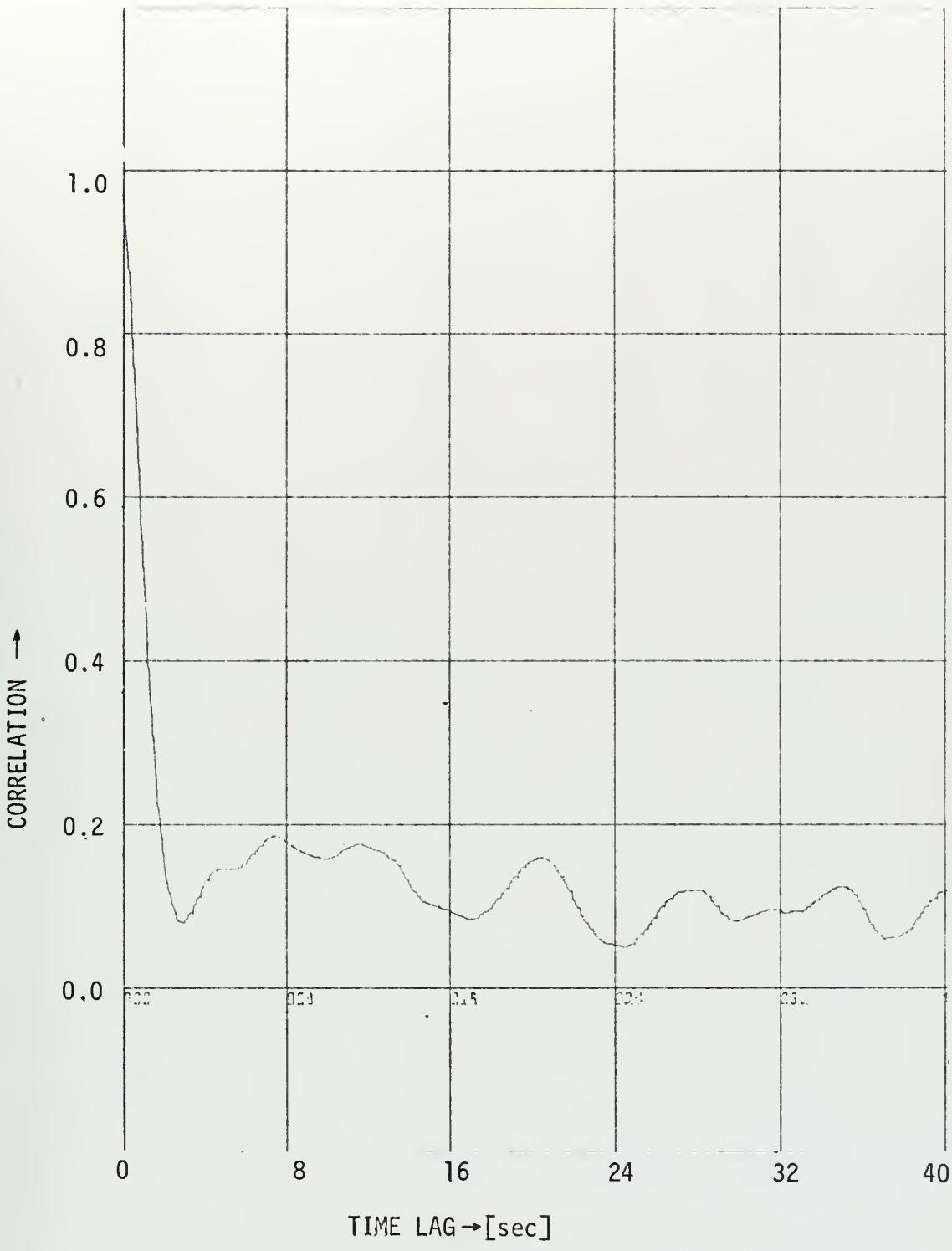

Fig. 25. Autocorrelation for Phase Modulation at 60 kHz

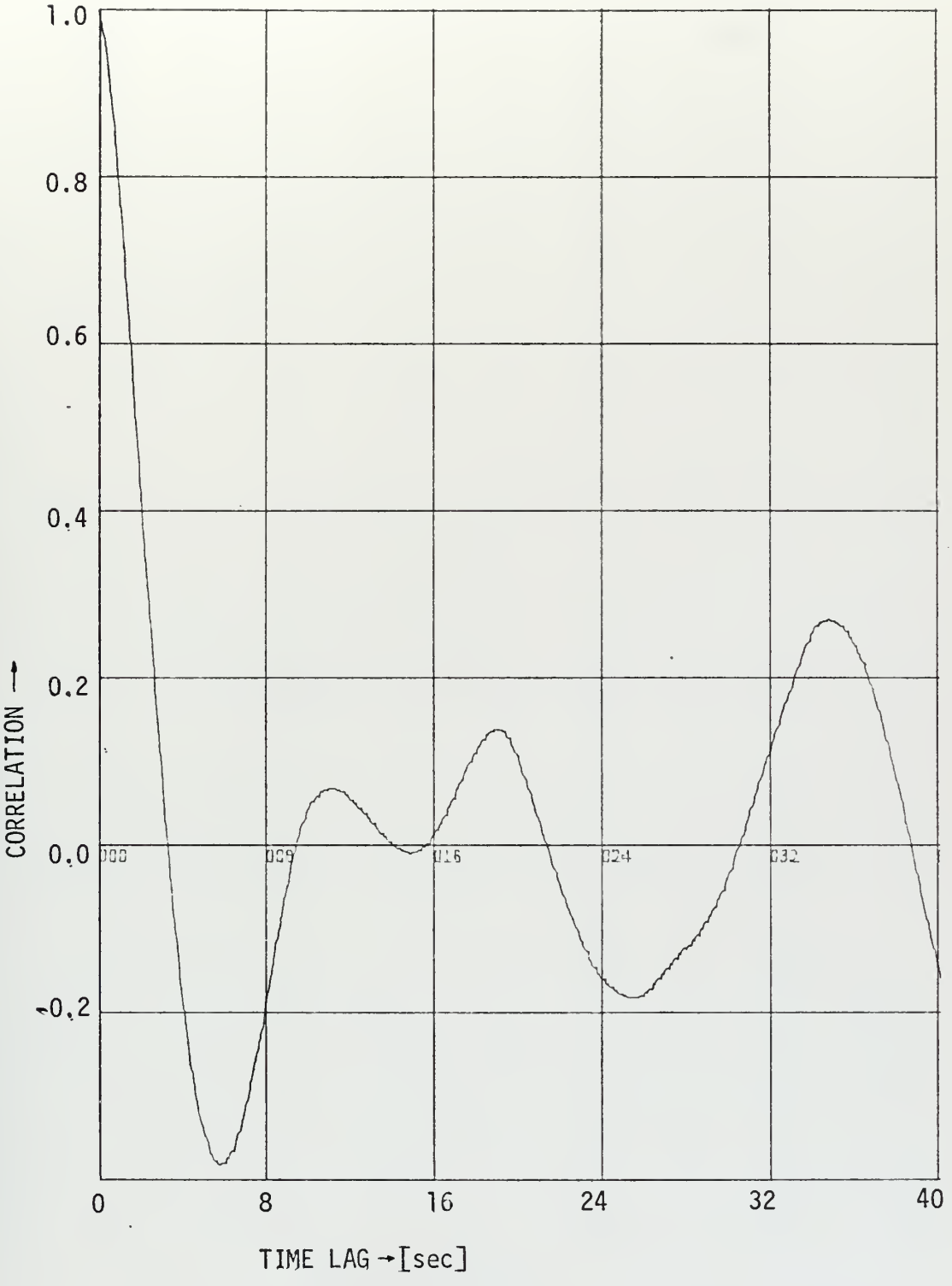

Fig. 26. Autocorrelation for Speed of Sound Fluctuations by Velocimeter

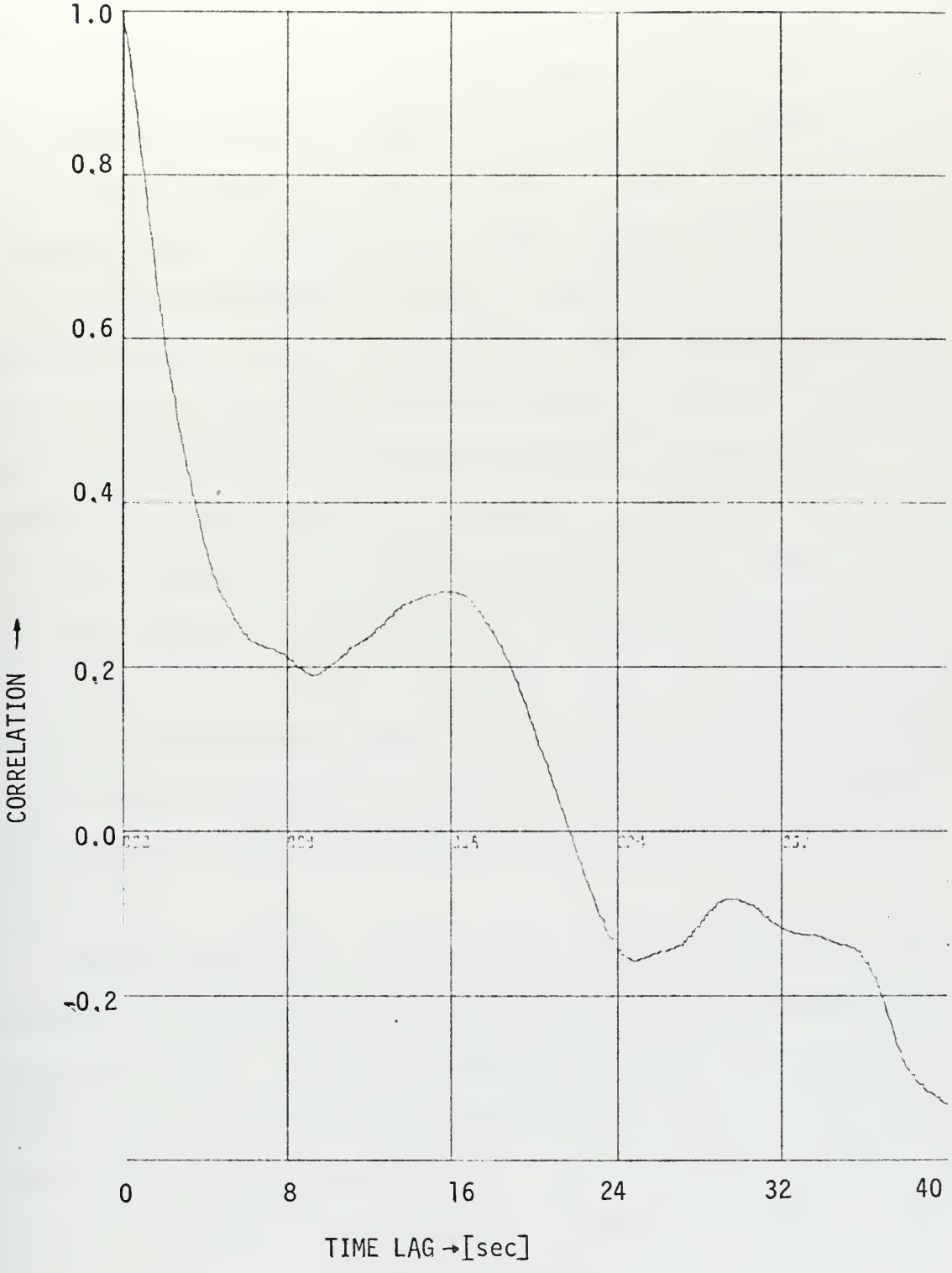

Fig. 27. Autocorrelation for Salinity Fluctuations

autocovariance by using a Parzen-lag-window. By taking the Fourier transform of this function one gets a smoothed power spectrum. The result of this computation using computer program (2) is a plot of phase angle squared per Hz versus frequency (The frequency resolution is .05 Hz. For better resolution in the amplitude, 10 $\log_{10}$ of the ordinate is taken such that the dimension is in dB). Several conclusions can be derived from the PSD-plot for the 4.3 m depth. For nearly all frequencies there is a distinct peak around .48 Hz probably due to the orbital effects caused by the observed predominant ocean wave component. From 0.5 to 2.5 Hz the values for the PSD follow an exponentially decaying curve. This pattern is interrupted by peaks mainly at .8, 1.3, 1.55, 1.95, and 2.35 Hz that may show up at two or at most three consecutive readings (see peak at 2.3 Hz in Figs. 28-31), or occur at one frequency and the next time two records later. Since every recording took two minutes this then suggests that the agency forcing these changes in the frequency spectrum is of a nature that can result in variations that show up only over a time period of four minutes or repeat every four minutes.

In general temperature, salinity, and/or bubble patches carried by turbulence and crossing the acoustical path could be the driving force for these variations. Since the sound signal integrates all these effects it is necessary to examine the temperature and salinity records. For the 20 min run and the depth of 4.3 m the power spectral density of the phase modulation with a frequency resolution of .0045 Hz, of the Ramsay velocimeter reading, and of the Bissett-Berman salinometer, all follow approximately the same exponentially decaying pattern, Figs. 31-33 (these graphs courtesy of LCDR Duchock and LT Seymour). The principal difference is that the PSD of the phase shows more power

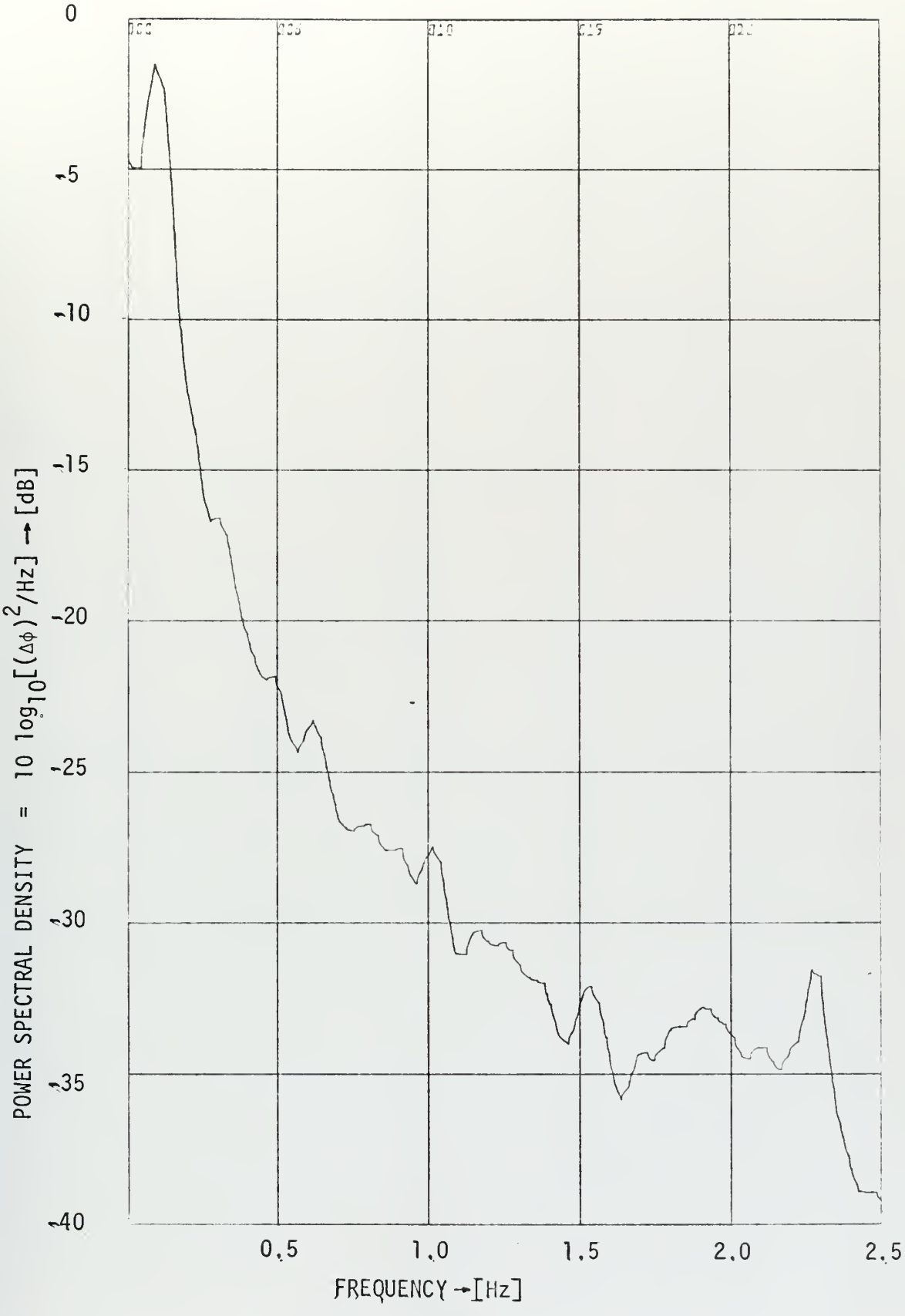

Fig. 28. Power Spectral Density, 46.4 kHz

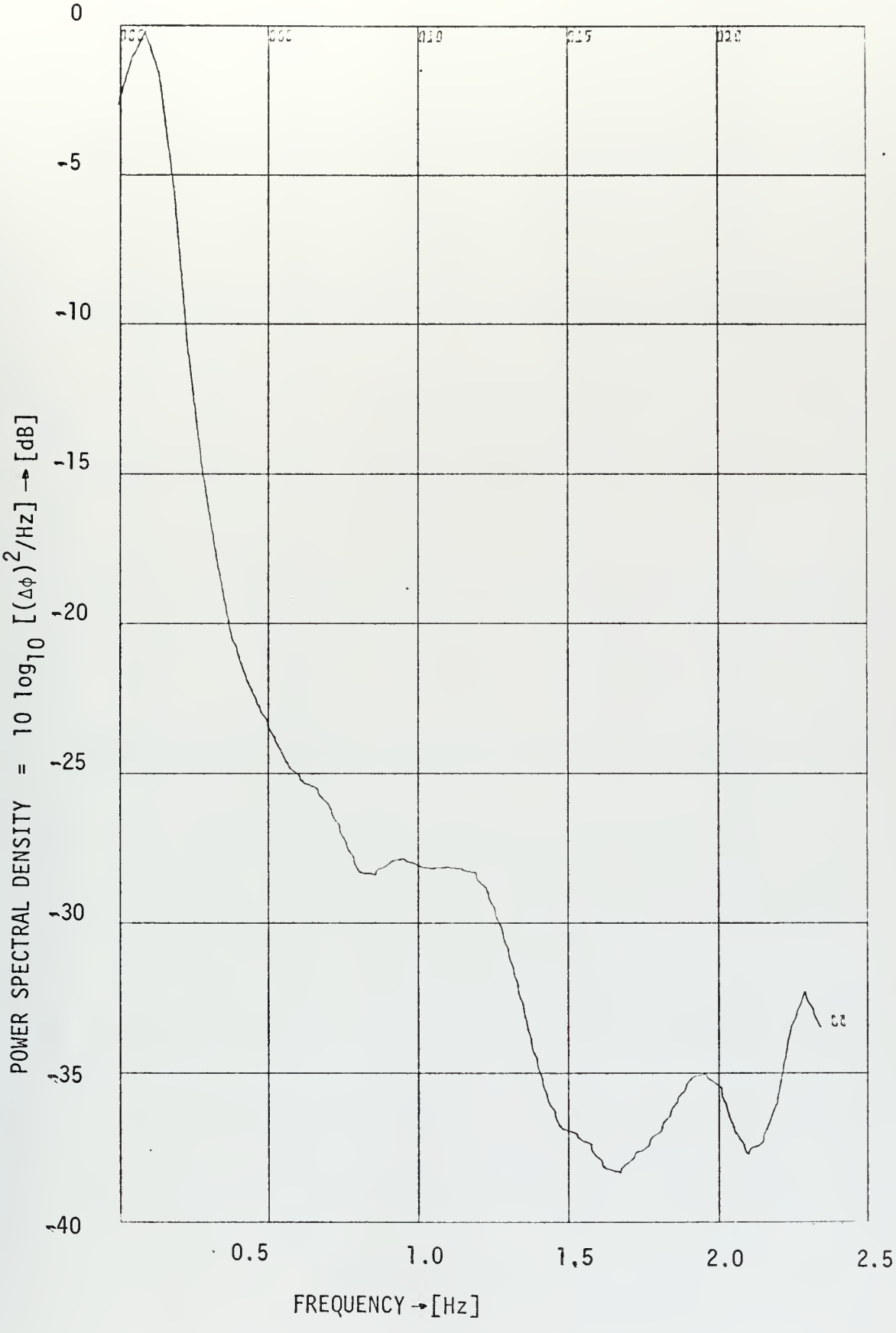

Fig. 29. Power Spectral Density, 48.4 kHz

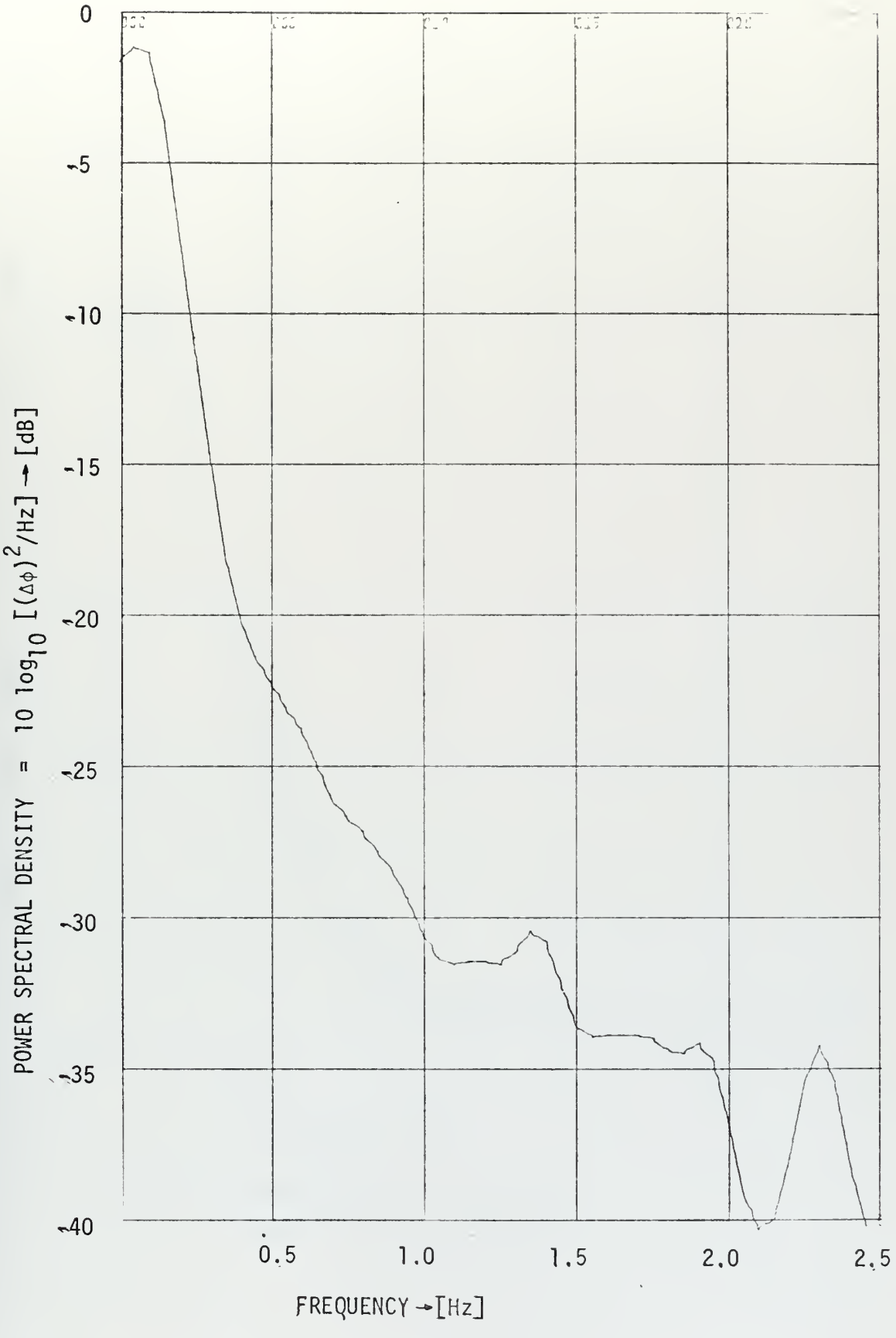

Fig. 30. Power Spectral Density, 50.3 kHz

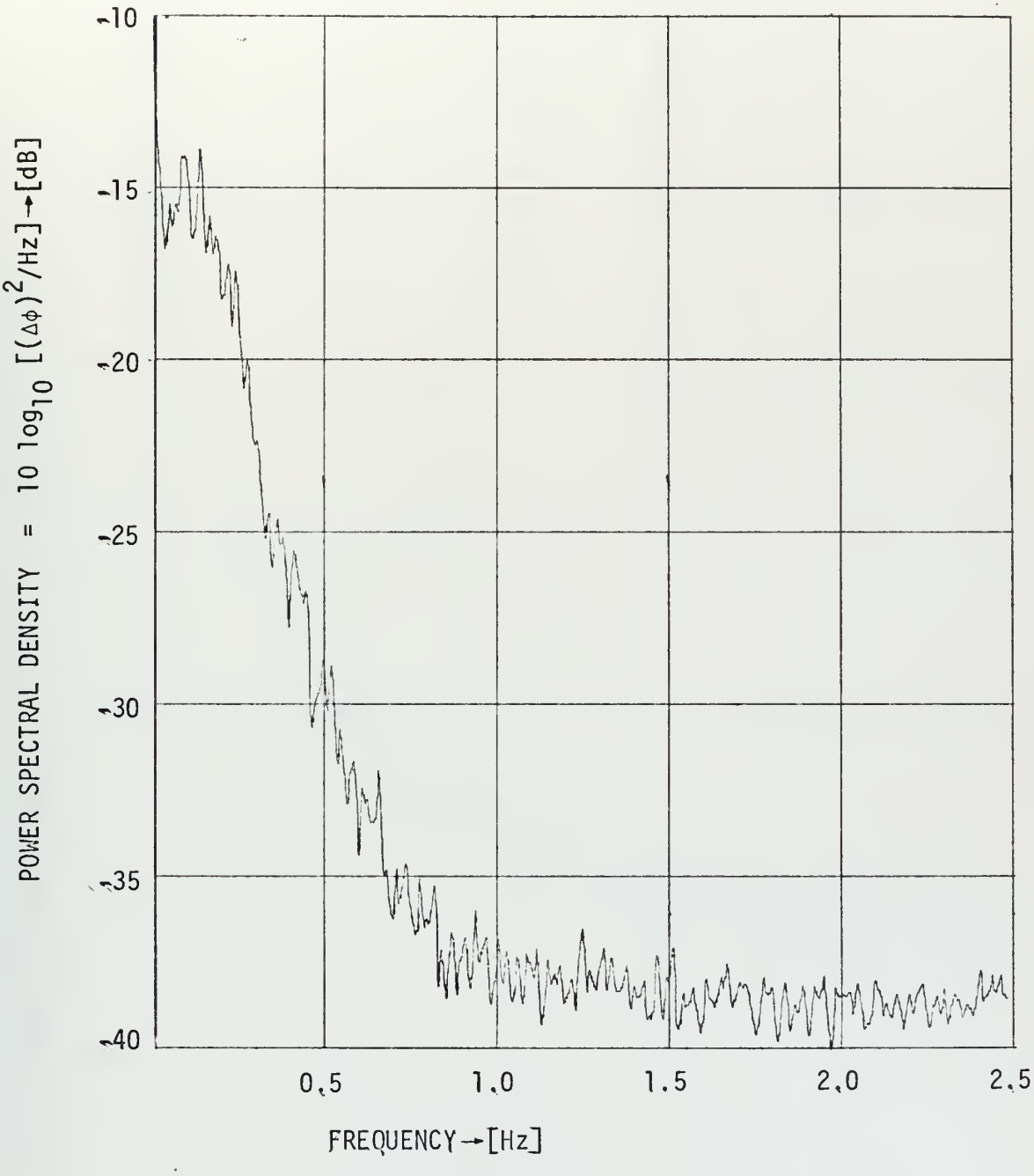

Fig. 31. Power Spectral Density for Phase Modulation at 60 kHz

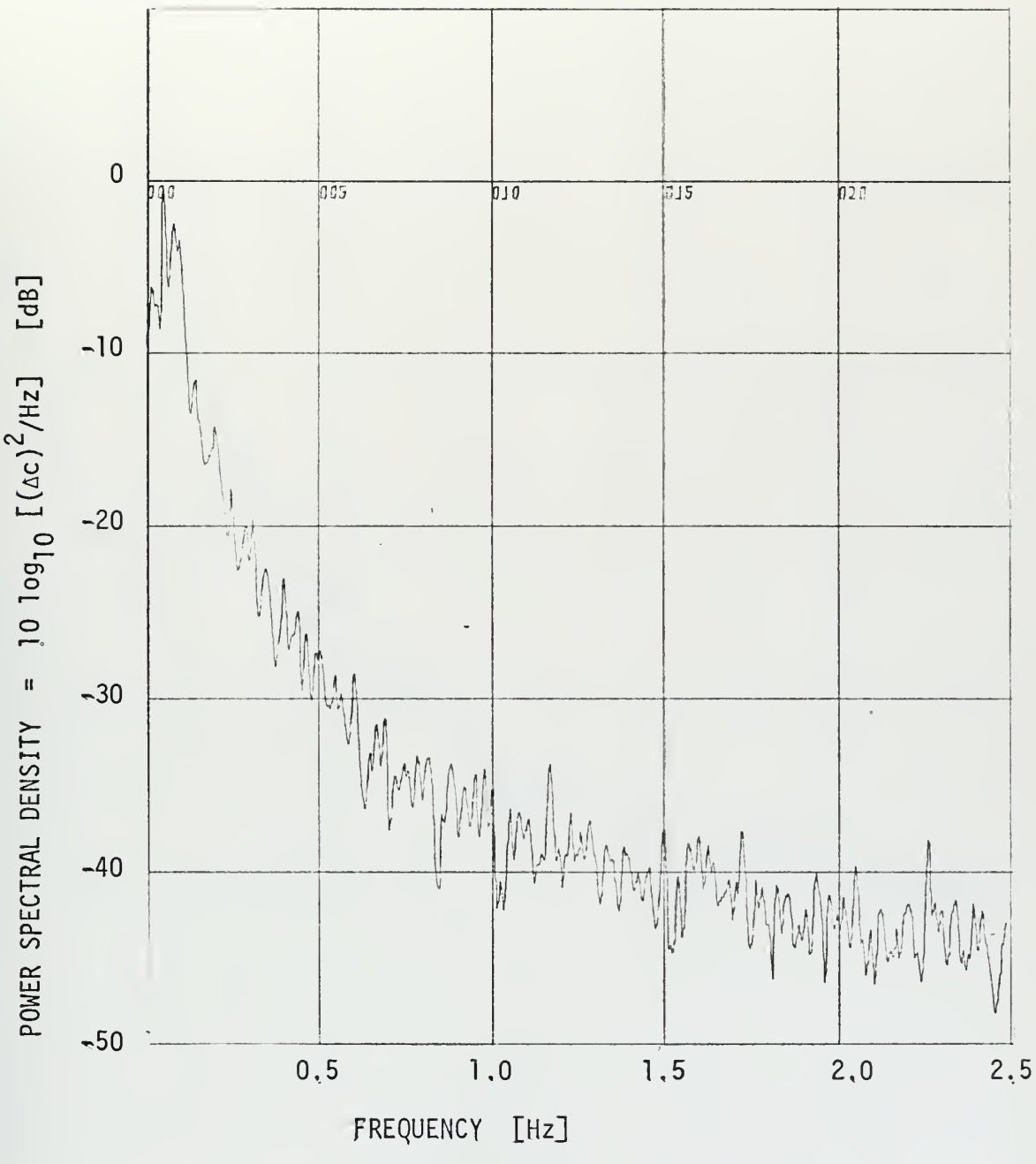

Fig. 32. Power Spectral Density for Speed of Sound Fluctuations by Velocimeter

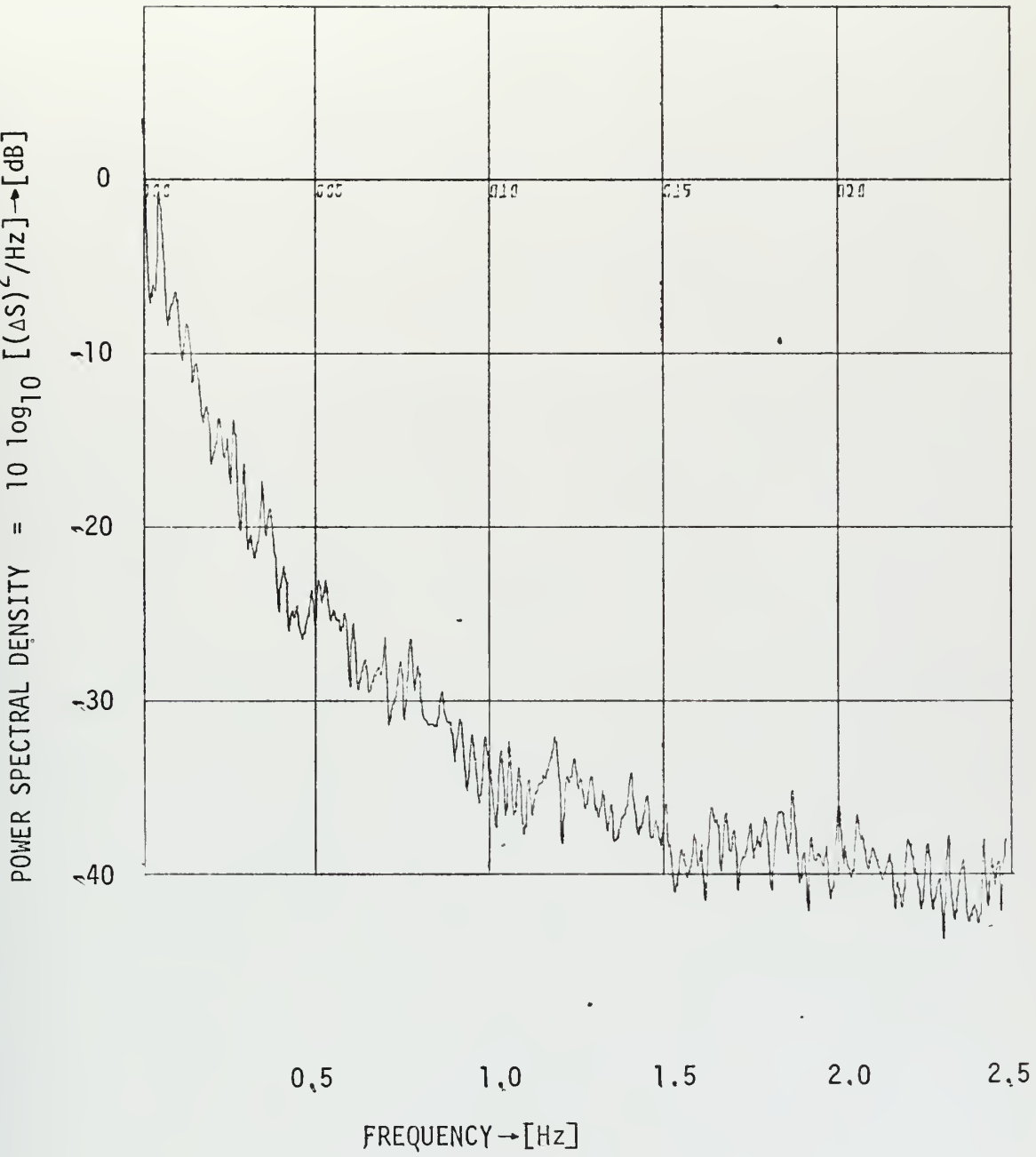

Fig. 33. Power Spectral Density for Salinity Fluctuations

concentrated below 0.5 Hz where orbital velocities are strong. All three plots of PSD show good agreement even in the fine structure in the range from 0.5 - 1.0 Hz.

X. ERROR ANALYSIS

The speed of sound as derived before is given by

$$c = \frac{fx}{\psi} = \frac{fx}{n \pm \phi/360}$$

In order to define the accuracy with which c is given we use the following approach:

$$\log c = \log f + \log x - \log (n \pm \phi/360)$$

$$\frac{dc}{c} = \frac{df}{f} + \frac{dx}{x} - \frac{d(n \pm \phi/360)}{n \pm \phi/360}$$

then the maximum error is given by

$$\frac{\Delta c}{c} = \frac{\Delta f}{f} + \frac{\Delta x}{x} + \frac{\Delta(n \pm \phi/360}{n \pm \phi/360}$$

This error will be calculated for the highest (80 kHz) and the lowest (30 kHz) frequencies. The coherent decade frequency synthesizer synthesizes the frequency of the output signal by proper combination of a number of frequencies, each derived on a proportional basis from a single internal master frequency crystal. It was essential in this application because of the requirement for a stable, sine-wave signal source capable of ultraprecise frequency adjustments through a wide frequency range. Since the output is always coherent in frequency with that of the quartz-crystal oscillator source it has the same percentage accuracy as the source which is essentially the smallest digit in the specific frequency or 1.6×10^{-7} at 60 kHz. This then implies that

$$\frac{\Delta f}{f} = \frac{10^{-2}}{30 \times 10^{3}} = 3.3 \times 10^{-7} \quad \text{at 30 kHz} \quad \text{and}$$

$$\frac{\Delta f}{f} = \frac{10^{-2}}{80 \times 10^{3}} = 1.25 \times 10^{-7} \quad \text{at 80 kHz}$$

Next the $\Delta x/x$ term will be examined. The absolute hydrophone distance could only be measured to one part in 1.5×10^{3} (0.5 mm) which is equivalent to

$$\frac{\Delta x}{x} = \frac{5 \times 10^{-4}}{.78} = 6.4 \times 10^{-4}$$

Assuming the $\Delta f/f$ and the $\Delta\psi/\psi$ terms to be zero this error in measuring the separation between the hydrophones results in an absolute error for the speed of sound of 1 m/sec (a level shift of 1 m/sec in the non-bubbly value of c), but does not affect the dispersion curve, that is the pattern of the speed of sound versus frequency. Therefore this error is no serious problem and will be ignored in the analysis since we are not interested in the absolute accuracy but rather the dispersion in the speed of sound.

To reduce possible errors due to changes in the geometrical configuration, especially in the separation distance between the hydrophones, it was necessary to use as a mounting a wire put under 100 lb of tension. The remaining possible vibration due to forces at sea was estimated to be 0.1 mm and results in

$$\frac{\Delta x}{x} = \frac{10^{-4}}{.78} = 1.28 \times 10^{-4}$$

The accuracy of the phase was the limiting factor. Since basically a phase interference approach was used to measure the speed of sound any relative phase changes could not be allowed to occur in the two arms of the system. It is a question whether one can assume the two parallel

parts within the system (hydrophone-preamplifier-filter-input channel phase meter) to be identical with respect to their influence on the signal. Actually, complete identity can never be obtained over a wide frequency range. Therefore special attention was given to the phase characteristic in selecting the hydrophones. The LC-5 resp. LC-10 were selected because their resonance is far above the frequency range of interest. Comparing the dispersion curve for 4.3 m with that at 14.3 m also points out that there is no phase variation in the pattern that shows up consistently at all depths and may therefore be due to a different phase behaviour of the two hydrophones. In addition the zero control of the phase meter has been used to compensate at a single frequency for unequal phase in the two receiving parts when the two input signals were known to be exactly in phase by using the electrical signal from the output of the frequency synthesizer.

The accuracy of the analog output of the phase meter is ±0.1°±0.3% of the phase angle measured for all frequencies or ±0.16° for the 20° phase angle which was used normally in the experiment. This causes a fractional error

$$\frac{\Delta(n \pm \phi/360)}{n \pm \phi/360} = \frac{.16}{(360 \times 16) + 20} = .272 \times 10^{-4} \text{ at 30 kHz}$$

$$= \frac{.16}{(360 \times 41) + 20} = .108 \times 10^{-4} \text{ at 80 kHz}$$

There are of course accuracy limitations in measuring the phase of distorted wave forms. Because the phase meter makes its phase measurements by measuring the fraction of a cycle between the negative-going zero axis crossing of the two test signals harmonic or scattered signals

can displace the zero crossing in either a plus or a minus manner depending on the phase relationship to the test signal.

The scattered signal was measured to be down by 37.4 dB re 1 V/μ bar as compared with the main signal which for the worst case could result in an error of .77°. A scattered signal a adding to the main signal b would result in the largest error in θ when the condition depicted below occurs

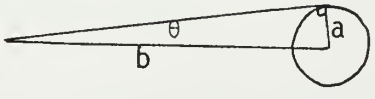

such that $20 \log \frac{b}{a} = 37.4$ dB

for small θ $\sin \theta \simeq \theta = \frac{a}{b}$

then $\frac{b}{a} = 10^{37.4/20} = 74$

and $\theta = \frac{1}{74} = .0135$ in radians

$\cong .77°$

A possible source of error is also the fact that at some frequencies the response of one hydrophone is significantly stronger than the other which means the possibility of harmonic content in the signal at multiples or submultiples of these frequencies. The limit error for a harmonic of magnitude, e, is $\theta = \frac{e}{a} 57°$ where a is the magnitude of the fundamental (manual for digital input phase meter model 355). Since the second harmonic was measured to be -46.34 dB re 1 V/μbar as compared with the fundamental the harmonic content could at most result in an error of 0.28°.

Assuming the worst condition for the phase reading or an error of .16° at the phase meter, a maximum additional error of .77° due to the

scattered signal, and also a maximum error of .28° due to harmonic content in the signal the total phase error could be

$$\frac{\Delta(n \pm \phi/360)}{n \pm \phi/360} = \frac{.16 + .77 + .28}{(360 \times 16) + 20} = 2.08 \times 10^{-4} \text{ at 30 kHz}$$

$$= \frac{1.207}{(360 \times 41) + 20} = .82 \times 10^{-4} \text{ at 80 kHz}$$

Summarizing it can be stated

$$\frac{\Delta c}{c} = 3.3 \times 10^{-7} + 1.28 \times 10^{-4} + 2.08 \times 10^{-4} = 3.36 \times 10^{-4} \text{ at 30 kHz}$$

$$= 1.25 \times 10^{-7} + 1.28 \times 10^{-4} + .82 \times 10^{-4} = 2.1 \times 10^{-4} \text{ at 80 kHz}$$

Therefore the maximum error in c is mainly determined by the percentage error in x and in ϕ and is given by

$$\Delta c = (1500)\ (3.36 \times 10^{-4}) = .5 \text{ m/sec at 30 kHz and}$$

$$= (1500)\ (2.1 \times 10^{-4}) = .31 \text{ m/sec at 80 kHz}$$

Comparing the value for Δc at the lower and at the upper limit points out that in general one is able to take more accurate measurements at the higher frequencies.

XI. SUMMARY AND CONCLUSIONS

A fixed source-hydrophone system separated by 1.8 m was used to study a) the in-situ speed of sound as a function of frequency and depth and b) the temporal characteristics of the phase fluctuations of a continuous wave acoustical signal over the frequency range 25 - 80 kHz. The experiment was carried out during Sea State 1 conditions at the NUC Oceanographic Research Tower in water of depth 56 ft one mile off shore at Mission Bay/San Diego in October 1971. The near surface region is of particular interest because bubbles and turbulence can have significant acoustical effects in addition to those caused by temperature and salinity inhomogeneities.

Four different depths, 4.3, 7.3, 9.3, and 14.3 m, were examined. The near surface values of c ranged from + 6 m/sec to -3 m/sec relative to the value for bubble-free sea water, with a maximum error of 0.5 m/sec. The speed of sound was found to peak at approximately 35 and 71 kHz at 4.3 m depth. The lower peak frequency increased as the depth is increased but not at the rate which would be expected for bubbles that are wind-initiated at the surface and carried to greater depths without losing their identity. A possible explanation is that the bubbles originated within the volume or at the bottom and lost gas by diffusion as they rose to the surface. Another possibility is that presence of more high frequency bubbles at the surface affects the apparent resonance frequency of the larger bubbles as determined by sound dispersion. The gradual and smooth drop-off in the resonant behaviour with increasing depth demonstrates that bubbles of this average size are somewhat continuously distributed in the medium down to 14.3 m. The

second distinct peak centered at 71 kHz appears to be only a characteristic of the shallowest run and does not repeat at the other depths. It is postulated that these small bubbles are introduced at the surface either by randomly breaking waves or by continental aerosols that drop into the water and carry tiny air bubbles with them (Medwin, 1970). The surface initiated bubbles disappear quite fast due to gas diffusion out of the bubble when transported downwards in the medium. We conclude from the foregoing that we encountered bubbles of radii centered around 124 and 54 microns and resonating at 30 and 69 kHz respectively. The broad dispersive characteristic around 30 kHz implies many bubbles larger than 60 microns whose principal source was at the surface and which were entrained by convective currents carrying them downwards.

Statistical analysis shows that for frequencies other than at the peak bubble populations the phase fluctuations can be approximated by a Gaussian probability density function. However around the peak variations in sound speed the PDF loses the smooth Gaussian appearance and shows a wide, somewhat irregular spread. The temporal variation of the standard deviation of the sound phase was small ($\pm$ .32°). However, the standard deviation of the phase fluctuation changed considerably as a function of frequency increasing to 1.92° at 40.6 kHz and to 2.56° at 70 kHz, the two sound dispersion centers of this experiment.

Typically, the phase was decorrelated (1/e) after 1.46 sec. This compares with preliminary oceanographic information which shows correlation times of 3.96 sec for the salinity and 2.28 sec for the speed of sound as measured by the velocimeter. These values show internal consistency.

The power spectral density of the varying phase shows its strongest values at frequencies less than 0.5 Hz; this is presumably due to bubbles entrained at orbital frequencies associated with the surface wave system which has maximum energy in the same frequency range.

Due to time considerations it was not possible to further examine the phase fluctuations in terms of the functional dependence on temperature, salinity, turbulence, and wave height. The analysis of the oceanographic parameters will be carried on in the theses by Lt. Bordy, LCDR Duchock, and Lt. Seymour (March 1972) and the emphasis should then be placed on the interrelation of the parameters as given by the cross-correlations or cross spectra for instance.

XII. RECOMMENDATIONS

It is recommended that research in this area be continued, especially by making an in-situ determination of the bubble concentrations at the same time as sound speed measurements are taken in order to determine the variation of bubble population with location, weather conditions, day or night, and local effects. It is also suggested to examine a smaller frequency range in more detail rather than to skim through a wide frequency range in larger steps and thereby losing valuable information. Frequencies below 30 kHz seem to be most inviting because of relevance to the Navy and promising because the largest changes in the speed of sound occur here, just below the frequency of the most prominent bubble population.

APPENDIX A. PRESENTATION OF DATA

Run 6, 4.3 m

freq [kHz]	real t [sec]	mean [Dig.]	standard dev. [Dig.]	mean [radians]	n	$c=\frac{fx}{n}$ x=.783
30.72	180	-.84	.06	-.07467	15.0987	1511.99
32.70	101	-.83	.08	-.07378	16.9096	1514.18
34.71	90	-.69	.06	-.06133	17.9220	1516.46
36.82	80	+.445	.11	+.03956	19.0562	1512.90
38.70	30	+.65	.08	+.05778	20.0745	1509.48
40.60	38	+.83	.12	+.07378	21.0905	1507.30
42.42	44	+.08	.08	+.00711	22.0238	1508.13
46.40	193	+.44	.06	+.03911	24.0558	1510.29
48.40	107	+.665	.06	+.05911	25.0758	1511.31
50.30	102	+.48	.06	+.04267	26.0593	1511.36
52.22	96	+.485	.03	+.04311	27.0598	1511.03
54.14	102	+.49	.06	+.04356	28.0602	1510.74
56.09	99	+.57	.06	+.05067	29.0673	1510.92
58.00	98	+.49	.06	+.04356	30.0602	1510.77
59.92	90	+.54	.06	+.04800	31.0647	1510.31
61.82	89	+.53	.06	+.04711	32.0638	1509.65
63.72	89	+.50	.07	+.04444	33.0611	1509.11
65.64	103	+.51	.11	+.04533	34.0620	1508.90
67.59	121	+.58	.11	+.05156	35.0682	1509.14
69.60	104	+.66	.14	+.05867	36.0753	1510.64
71.56	86	+.65	.10	+.05778	37.0745	1511.32
73.49	90	+.70	.11	+.06222	38.0789	1511.14
75.38	101	+.59	.09	+.05244	39.0691	1510.72
77.28	110	+.56	.07	+.04978	40.0665	1510.25
79.20	78	+.57	.07	+.05067	41.0673	1510.05

Run 7, 4.3 m

freq [kHz]	real t [sec]	mean [Dig.]	standard dev. [Dig.]	mean [radians]	n	$c=\frac{fx}{n}$ x=.783
30.69	73.6	-.94	.06	-.0836	15.8997	1511.37
32.69	112.8	-.85	.04	-.0756	16.9077	1513.88
34.69	113.6	-.87	.05	-.0773	17.9060	1516.94
36.60	88.0	-.97	.04	-.0862	18.8971	1516.52
38.76	98.4	+.65	.09	+.0578	20.0745	1511.82
40.61	93.6	+.43	.07	+.0382	21.0549	1510.22
40.61	93.6	+.44	.07	+.0391	21.0558	1510.16
42.53	104.8	+.53	.05	+.0471	22.0638	1509.30
44.45	93.6	+.47	.04	+.0418	23.0585	1509.39
48.34	88.8	+.55	.05	+.0489	25.0656	1510.05
52.19	92.8	+.56	.06	+.0498	27.2667	1509.79
56.04	104.8	+.48	.06	+.0427	29.0594	1509.99
59.86	78.4	+.45	.09	+.0400	31.0567	1509.19
63.66	99.2	+.51	.09	+.0453	33.0620	1507.65
67.50	99.2	+.47	.07	+.0418	35.0585	1507.55
71.44	73.6	+.52	.09	+.0462	37.0629	1509.26
75.24	92.0	+.50	.08	+.0444	39.0611	1508.22
79.10	105.6	+.51	.07	+.0453	41.0620	1508.34

Run 8, 9.3 m

freq [kHz]	real t [sec]	mean [Dig.]	standard dev [Dig.]	mean [radians]	n	$c=\frac{fx}{n}$ x=.783
25.17	81.6	+.51	.03	+.0453	13.062	1508.81
28.98	79.2	+.60	.03	+.0533	15.070	1505.73
32.91	84.8	+.56	.05	+.0498	17.0665	1509.89
36.79	96.0	+.46	.03	+.0409	19.0576	1511.55
40.62	91.2	+.54	.03	+.0480	21.0647	1509.89
44.49	93.6	+.57	.06	+.0507	23.0674	1510.17
48.34	102.4	+.59	.07	+.0524	25.0691	1509.84
52.18	95.2	+.59	.04	+.0524	27.0691	1509.36
56.07	103.2	+.51	.10	+.0453	29.0620	1510.66
59.94	88.8	+.58	.08	+.0516	31.0683	1510.64
63.71	101.6	+.48	.08	+.0427	33.0594	1508.95
67.56	108.0	+.49	.07	+.0436	35.0603	1507.92
71.39	54.4	+.46	.05	+.0409	37.0576	1508.42

Run 9, 14.3 m

freq [kHz]	real t [sec]	mean [Dig.]	standard dev. [Dig.]	mean [radians]	n	$c=\frac{fx}{n}$ x=.783
28.95	42.4	+.70	.05	+.0622	15.0789	1503.28
36.76	28.0	+.62	.08	+.0551	19.0718	1509.20
44.48	32.0	+.56	.04	+.0498	23.0665	1509.89
55.93	36.8	+.58	.06	+.0516	29.0683	1506.56
59.78	36.8	+.54	.05	+.0480	31.0647	1506.78
63.57	25.6	+.53	.06	+.0471	33.0638	1505.43
71.28	78.4	+.76	.09	+.0676	37.0843	1505.01

Run 10, 7.3 m

freq [kHz]	real t [sec]	mean [Dig.]	standard dev. [Dig.]	mean [radians]	n	$c=\frac{fx}{n}$ x=.783
27.05	81.6	.59	.04	.0524	14.0691	1505.44
30.96	71.2	.70	.05	.0622	16.0789	1507.67
34.89	96.8	.51	.04	.0453	18.0620	1512.51
38.72	89.6	.55	.04	.0489	20.0656	1510.93
42.55	87.2	.61	.04	.0542	22.0709	1509.53
46.40	89.6	.56	.05	.0498	24.0665	1509.62
50.23	81.6	.57	.09	.0507	26.0674	1508.78
54.09	86.4	.52	.05	.0462	28.0629	1509.20
57.70	84.8	-1.08	.07	-.0960	29.8873	1511.65
61.59	80.0	-.79	.06	-.0702	31.9131	1511.13
65.59	78.4	.48	.13	.0427	34.0594	1507.86

```
C       PROGRAM 1
C       PROGRAM CONVERT(INPUT,OUTPUT,PUNCH)
C       AVGX IS THE AVERAGE DISTANCE DISTANCE THE RECORDING
C       DRUM ADVANCES PER ONE HOUR REAL TIME, I.E. THE DATA
C       SAMPLING RATE,
        DIMENSION U(6000),V(6000),N(80),IBUFF(5000),NK(80)
        IK=0
        READ 97,L
    97  FORMAT(I2)
        READ 98,AVGX
    98  FORMAT(F10.0)
        READ 96,IFILE
    96  FORMAT(I2)
        DO 116 JJ=1,L
        DELT=36.0/AVGX
        PRINT 99,DELT
    99  FORMAT(1H0,2X,25H SAMPLING INTERVAL EQUALS, 1X,E15.7,
       11X,7HSECONDS)
        PRINT 700,JJ
   700  FORMAT(1H0,9HJJ EQUALS, 2X,I2)
        DO 100 I=1,5500
        U(I)=0.0
   100  V(I)=0.0
   101  DO 202 I=1,5000
   202  IBUFF(I)=0
        COUNTX=0.0
        COUNTY=0.0
        NUM=5000
        M=1
        K8=0
        CALL LIOF(5LRBCD1,IBUFF,NUM,NPAR,NEOF)
        IF(NEOF) 602,200
   200  K=-7
        KF=0
   201  K=K+8
        KA=K+8
        KC=0
        DO 102 KB=K,KA
        KC=KC+1
        NK(KC)=IBUFF(KB)
   102  IF (NK(KC).EQ.0) KF=1
        DECODE(80,103,NK) (N(I),I=1,80)
   103  FORMAT(80R1)
        DO 104 I9=1,80
        IF(N(I9).EQ.50B) GO TO 106
        IF(N(I9).EQ.55B) GO TO 107
        IF(N(I9).EQ.34B) GO TO 108
C       SYMBOL / (50) REPRESENTS AN INCREMENT TRAVEL IN THE
C       MINUS X OR Y DIRECTION BY THE DIGITIZER.
C       SYMBOL 0,(55B), REPRESENTS A ZERO INCREMENT TRAVEL
C       IN THE X OR Y DIRECTION BY THE DIGITIZER
C       SYMBOL 1,(34B), REPRESENTS AND INCREMENT TRAVEL IN
C       THE POSITIVE X OR Y DIRECTION BY THE DIGITIZER
C       SYMBOL *,(47B), IS A FLAG INSERTED IN IN THE RECORD
C       BY THE PERSON DIGITIZING BY USE OF THE IRG
        GO TO 104
   106  RX=-0.01
        K8=K8+1
        GO TO 109
   107  RX=0.0
        K8=K8+1
        GO TO 109
   108  RX=0.01
        K8=K8+1
   109  K3=K8/2
        K3=2*K3
        IF(K3.EQ.K8) GO TO 111
        COUNTX=COUNTX+RX
        IF(COUNTX.NE.0.0) GO TO 110
        GO TO 104
   110  U(M)=COUNTX
        GO TO 104
```

```
  111 COUNTY=COUNTY+RX
      IF(COUNTX.NE.0.0) GO TO 112
      GO TO 104
  112 V(M)=COUNTY
      COUNTX=0.0
      M=M+1
      IF(M.GT.6000) GO TO 600
  104 CONTINUE
      IF(KF.EQ.1) GO TO 113
      GO TO 201
  113 MAX=M-7
  105 PRINT 205,M,I9
  205 FORMAT(1H0,2I10)
C     TOTAL TIME OF THE RECORD EQUALS NUMBER OF DATA
C     POINTS TIMES THE SAMPLING INTERVAL, DELT.
      TIME=(M*DELT)/3600.0
      PRINT 115,TIME
  115 FORMAT(1H,10X,28H TOTAL TIME OF RECORD EQUALS,2X,
     1E15.7,2X,7H HOURS.)
      PRINT 215,(V(I),I=1,M)
      PRINT 215,(U(I),I=1,M)
  215 FORMAT(1H ,10X,14F7.2)
      PUNCH 213,(V(I),I=1,M)
  213 FORMAT(14F5.2)
      PUNCH 2100
 2100 FORMAT (20H********************)
  116 CONTINUE
      STOP
  600 PRINT 601
  601 FORMAT(1H0,20X,37H***** U AND V SPACE INADEQUATE ***,)
  602 IK=IK+1
      IF(IK.GT.IFILE)603,200
  603 STOP
      END
```

```
C       PROGRAM 2
C       PROGRAM FOR THE SPECTRAL ANALYSIS OF APERIODIC RECORDS
C       DATA MUST BE SAMPLED AT EQUAL INTERVALS OF DT
C       CALCULATES EITHER THE AUTO SPECTRA OR THE CROSSSPECTRA
C       IF NFLAG1=0 , AUTOSPECTRA.....IF NFLAG1=1    COSPECTRA
C       IF NFLAGP = 1 ..... CALL PRESS, TOTE
C        IF NFLAGC = 1 .....CALL URMS
C  NTS= NUMBER OF TIME SAMPLES
C  MLAG = NUMBER OF TIME LAGS
C  DT = TIME INCREMENT
C  DHZ = FREQUECY SPACING
C  FBHZ = LOWEST FREQUENCY (HZ)
C  FEHZ = HIGHEST FREQUENCY OF INTEREST (HZ)
C  TM =DT*MLAG
C  DHZ = 1/(2*A*TM)
C  FEHZ = B/(2*TM)= B/(2*MLAG*DT)
C  FEHZ = A*B*DHZ
C  A*B = TOTAL NO. FREQUENCY SPACINGS OF ENERGY SPECTRUM
C  A AND B ARE INTE&ER CONSTANTS
C  TRANS-- INSTRUMENT AND REMARKS
       REAL*8 ITITLE(12),ITITEL(12),ITITIL(12)
       DIMENSION F1(6000),F2(6000)
       DIMENSION PHI(600),TAU(600),SPHI(600),APHI(600),
      1PHN(600)
       DIMENSION FREQ(700),CYCL(700),SPEC(700),SSP(700)
       DIMENSION CSPEC(700),QSPEC(700),SS2(700)
       DIMENSION RESPF(700),PER(700),SPE2(700),PHASE(700),
      1COHER(700)
       DIMENSION DATE(2),HOUR(2),TRANS(10)
       REAL*4 LABEL/4H CO /,LABLI/4HQUAD/,MONT,LABIL/4H PHI/,
      1LABLE/4HCROS/
       READ(5,200,END=888) (ITITLE(I),I=1,12)
       READ(5,200,END=888) (ITITEL(I),I=1,12)
   200 FORMAT(6A8)
       READ(5,802) DATE,HOUR,TRANS
   802 FORMAT(2A4,2A4,10A4)
       READ(5,96) NFLAG1,NFLAGP,NFLAGC
       READ(5,99) NTS,MLAG,DT,DHZ,FBHZ,FEHZ
       READ(5,801) CALX1,CALX2,H,X2,AZZ,S
       WRITE(6,811)
   811 FORMAT(1H1)
       WRITE(6,803) DATE,HOUR,TRANS
       WRITE(6,98) NTS,MLAG,DT,DHZ,FBHZ,FEHZ,CALX1,CALX2,H,X2
    96 FORMAT (3I6)
    98 FORMAT(7H NTS = ,I6//,8H MLAG = ,I6//,6H DT = ,F9.5//,
      16H DHZ= ,F10
      2.8//,' FBHZ = ',F10.8//,' FEHZ = ',F12.8//,' CALX1 = '
      3,F10.8//,
      4' CALX2 = ',F10.8//,' H = ',F10.3//,' X2 = ',F10.3//)
    99 FORMAT (2I6,5F10.8)
   801 FORMAT(6F10.5)
   803 FORMAT(40H SOUND PHASE STUDY OF SAN DIEGO BAY     ,
      15X,7H DATE  ,2A4,10H   HOUR   ,2A4//,5X,10A4///)
C  BAND WIDTH FREQUENCIES OF TOTAL ENERGY FLUX- CMIN,CMAX
       CMIN = 0.0
       CMAX = 0.2
C
C  COMPUTING POWER SPECTRUM
       PI=3.14159265
       FB = FBHZ*2.0*PI
       FE = FEHZ*2.0*PI
       DF = DHZ *2.0*PI
       FMIN = 2.0*PI*CMIN
       FMAX = 2.0*PI*CMAX
   900 FORMAT(14F5.2)
       READ(5,900)(F1(I),I=1,NTS)
       XMAX = F1(1)
       DO 23 I=2,NTS
       IF(XMAX.GE.F1(I)) GO TO 23
       XMAX = F1(I)
    23 CONTINUE
       DO 24 I=1,NTS
```

```
      F1(I)=(F1(I)-XMAX)
   24 CONTINUE
      WRITE(6,901)(F1(I),I=1,NTS)
  901 FORMAT(14F7.2)
      CALL TREND(F1,NTS,DT,CALX1)
   21 DO 10 M=1,MLAG
      SUM=0.0
      NMAX=NTS-M+1
      DO 8 I=1,NMAX
      NN=M+I-1
    8 SUM=SUM+F1(I)*F1(NN)
      XNMAX=NMAX
      XX=M-1
      TAU(M)=XX*DT
      PHI(M)=SUM/XNMAX
      PHN(M) = PHI(M)/PHI(1)
   10 CONTINUE
      CALL PARZ(MLAG,PHI)
  798 FORMAT(' PHI(0) = ',F10.4//)
      NFREQ=(FE-FB)/DF+0.1
      DO 14 N=1,NFREQ
      XN=N
      FREQ(N)=(XN-1.0)*DF+FB
   14 CYCL(N) = FREQ(N)/(2.0*PI)
      PER(1) = 0.0
      DO 15 N = 2,NFREQ
   15 PER(N) = 1.0/CYCL(N)
      MLAGM1=MLAG-1
      XMLAG=MLAG
   46 DO 50 N=1,NFREQ
      SUM=0.5*(PHI(1)+PHI(MLAG)*COS(FREQ(N)*TAU(MLAG)))
      C1=COS(FREQ(N)*DT)
      S1=SIN(FREQ(N)*DT)
      CC=1.0
      SC=0.0
      DO 49 M=2,MLAGM1
      CT=CC*C1-SC*S1
      ST=SC*C1+CC*S1
      CC=CT
      SC=ST
   49 SUM=SUM+PHI(M)*CC
   50 SPEC(N)=SUM*2.0/XMLAG
      IF(NFLAGP) 741,741,742
  742 CONTINUE
      CALL PRESS(FREQ,SPEC,NFREQ,H,X2,DF,FB,FMAX)
  741 CONTINUE
      MD=3.14159265/(DF*DT*XMLAG)+0.1
      DC = DF/(2.0*PI)
      SUM = 0.0
      DO 650 N=1,NFREQ
  650 SUM = SUM + SPEC(N)
      WRITE(6,651) SUM
  651 FORMAT (25H      VARIANCE OF SPECTRUM//,3X,
     116H      VARIANCE = ,F10.5,10H    M2      //)
      WRITE(6,106)(TAU(M),PHN(M),M=1,MLAG)
      INUM=FEHZ/DHZ
      DO 9988 I=1,INUM
      SPEC(I)=10*ALOG10(SPEC(I))
 9988 CONTINUE
C     CALL DRAW TO PLOT SPECTRUM OF SAN DIEGO
C     AS A FUNCTION OF FREQUENCY
      CALL DRAW(200,TAU,  PHN,0,0,LABEL,ITITEL,8.0,0.0,2,0,2
     1,0,8,8,1,LAST)
      CALL DRAW(INUM,CYCL,SPEC,0,0,LABEL,ITITLE,0.0,0.0,0,0,
     10,0,8,8,1,LAST)
  105 FORMAT (10X,24H ENERGY SPECTRAL DENSITY///,5X,
     110H FREQUENCY,5X,13H
     2 RAW SPECTRUM,3X,18H SMOOTHED SPECTRUM//)
  106 FORMAT (5X,F10.5,6X,F10.5)
      WRITE(6,105)
      WRITE(6,106)(CYCL(M),SPEC(M)        ,M=1,NFREQ)
  888 RETURN
```

```
      END

      SUBROUTINE PRESS(FREQ,SPEC,NFREQ,H,X2,DF,FB,FMAX)
C SUBROUTINE TO CONVERT PRESSURE SPECTRUM TO ENERGY SPECTRUM
      DIMENSION FREQ(NFREQ),SPEC(NFREQ)
      NMAX = (FMAX-FB)/DF+1.0
      DO 11 I=1,NMAX
C CALCULATE LINEAR WAVE LENGTH BY NEWTONS METHOD
      IF(FREQ(I)-0.00001) 8,8,7
    7 XKHO = FREQ(I)*FREQ(I)*H/9.80
      IF(XKHO-6.3) 5,1,1
    1 XKH = XKHO
      GO TO 9
    5 XKH = SQRT(XKHO)
    3 SH = SINH(XKH)
      CH = COSH(XKH)
      EPS = XKHO-XKH*SH/CH
      SLOPE = -XKH/CH**2-SH/CH
      DXKH = -EPS/SLOPE
      IF(ABS(DXKH/XKH)-0.0001) 9,9,4
    4 XKH = XKH+DXKH
      GO TO 3
    8 RESPF = 1.00
      GO TO 11
    9 XK = XKH/H
      RESPF = COSH(XK*H)/(COSH(XK*(H-X2)))
      IF(RESPF-10.0) 11,11,12
   11 SPEC(I) = RESPF*RESPF*SPEC(I)
   12 RETURN
      END

      SUBROUTINE TREND(FX,NTS,DT,CALXX)
      DIMENSION FX(NTS)
C CALIBRATIONG RECORD
      DO 104 I=1,NTS
  104 FX(I) = FX(I)*CALXX
C COMPUTING THE LINEAR TREND
      FNTS = NTS
      SUMF = 0.0
      DO 101 I=1,NTS
  101 SUMF = SUMF + FX(I)
      SUMF1 = 0.0
      DO 102 I=1,NTS
      XI = I
  102 SUMF1 = SUMF1 + XI*FX(I)
      XNM1 = NTS-1
      XNP1 = NTS+1
      XM = (1.0/DT)*(12.0*SUMF1/(FNTS*XNM1*XNP1)-6.0*SUMF/
     1(XNM1*FNTS))
      B = SUMF/FNTS-XM*XNP1*DT/2.0
      FMEAN = SUMF/FNTS
      WRITE(6,9) FMEAN,XM,B
    9 FORMAT (3X,8H MEAN = ,F10.5,3X,9H SLOPE = ,F10.5,3X,
     113H INTERCEPT= ,F10.5//)
      DO 103 I=1,NTS
      XI = I
  103 FX(I) = FX(I) - (B+XM*XI*DT)
      RETURN
      END

      SUBROUTINE SMO(MD,X1,X2,NFREQ)
      DIMENSION X1(MD),X2(MD)
      DO 1 N=1,MD
      NA=N+MD
      NN=NFREQ-N+1
      NB=NN-MD
      X2(N) = 0.25*(X1(1)+X1(NA))+0.5*X1(N)
    1 X2(NN)=0.5*(X1(NN)+X1(NB))
    3 MB=MD+1
```

```
      ME=NN-1
    5 DO 2 N=MB,ME
      NA=N+MD
      NB=N-MD
    2 X2(N)=0.25*(X1(NA)+X1(NB))+0.5*X1(N)
      RETURN
      END

      SUBROUTINE PARZ(MLAG,PHI)
C     PARZ SUBROUTINE PARZEN FILTERS AUTO-CORRELLATION FUNCT
      DIMENSION PHI(MLAG)
      XMLAG = MLAG
      MLAGH = XMLAG/2.0-0.1
      MLAGH1 = MLAGH + 1
      DO 31 M=1,MLAGH
      MM = M-1
      R = MM
      RM = R/XMLAG
      UM = 1.0-6.0*RM*RM*(1.0-RM)
      PHI(M ) = PHI(M )*UM
   31 CONTINUE
      DO 32 M = MLAGH1,MLAG
      MM = M-1
      R = MM
      RM = R/XMLAG
      RM1 = (1.0-RM)
      UM = 2.0*RM1*RM1*RM1
      PHI(M ) = PHI(M )*UM
   32 CONTINUE
      RETURN
      END
```

```
C      PROGRAM 3 CALCULATES DISPERSION IN C
//   EXEC FORTCLGP,REGION.GO=100K
//FORT.SYSIN DD *
       REAL*8 TITLE(12)/'BOX 209 ',11*'          '/
       REAL LABEL/'    '/
       DIMENSION A(10),B(10),MR(10),W(500),CC(500)
       DATA PI/3.1415926/
C SET MAX DIMENSION TO WORK WITH.
       NOUT=500
C READ PZ,RHZ,CZ.
       READ(5,100) PZ,RHZ,CZ
  100  FORMAT(3F10.5)
       PZ=PZ*100000.0
C READ RADIUS (MICRONS) AND FREQ.
       READ(5,200) ISR,IDR,IER,ISW,IDW,IEW
  200  FORMAT(6I10)
C READ NO. OF SEGMENTS AND THEIR VALUEX...MAX OF 10 SEGMENTS
       READ(5,300) NS
  300  FORMAT(I2)
       READ(5,400)(A(I),B(I),MR(I),I=1,NS)
  400  FORMAT(2F10.5,I10)
C PRINT INPUT.
       WRITE(6,500)
  500  FORMAT('1INPUT:')
       WRITE(6,510) PZ,RHZ,CZ
  510  FORMAT(' PO = ',E16.8,T28,'RHO = ',E16.8,T54,'CO = ',
      1E16.8)
       WRITE(6,520) ISR,IDR,IER
  520  FORMAT(' STARTING RADIUS = ',I6,T28,'INCREMENT = ',I3,
      1T54,'ENDING RADIUS = ',I6)
       WRITE(6,530) ISW,IDW,IEW
  530  FORMAT(' STARTING W = ',I6,T28,'INCREMENT = ',I3,T54,
      1'ENDING W = ',I6)
       WRITE(6,540)
  540  FORMAT('    SEGMENT',7X,'A',15X,'B',9X,'MAX. RADIUS')
       WRITE(6,550) (I,A(I),B(I),MR(I),I=1,NS)
  550  FORMAT(5X,I2,3X,E16.8,2X,E16.8,4X,I6)
C CHECK FOR INPUT ERROR. MR SHOULD INCREASE.
       NJ=NS-1
       IF (NJ .EQ. 0) GO TO 700
       DO 600 J=1,NJ
       IF (MR(J) .LT. MR(J+1)) GO TO 600
       WRITE(6,560)
  560  FORMAT(' SEGMENT RADII ARE OUT OF SEQUENCE.')
       STOP
  600  CONTINUE
C NOW CALCULATE SOME CONSTANTS TO SAVE TIME.
  700  IR=(IER-ISR)/IDR+1
       IW=(IEW-ISW)/IDW+1
       WC=1.975*SQRT(PZ/RHZ)*1000000.0
       PIC=0.027/((PI*2000.0)**0.322)
C CLEAR OUTPUT BUFFER
       DO 800 I=1,NOUT
       W(I)=0.
  800  CC(I)=0.
C INITIALIZE STARTING VALUES.
C WW=WORKING OMEGA.
C WZI=CALCULATED OMEGA ZERO SUB I.
C RW=WORKING RADIUS.
       ITEMPW=ISW
       DO 2000 K=1,IW
       WW=ITEMPW
       W(K)=ITEMPW
       IF (K.NE.1) GO TO 915
       WRITE(6,900) ITEMPW
  900  FORMAT('1W = ',I6)
       WRITE(6,910)
  910  FORMAT('    INDEX',6X,'RADIUS',11X,'WZ',13X,'U(R)D(R)')
  915  SUM=0.0
       ITEMPR=ISR
C THIS IS THE SUMMATION LOOP.
       DO 1000 L=1,IR
```

```
      WZI=WC/ITEMPR
      DI=PIC*(WZI**0.322)
      WRAT=WZI/(WW*2.0*PI*1000.0)
      WRAT2=WRAT*WRAT
      WRATM=WRAT2-1.0
      BATH=WRATM/((WRATM*WRATM)+(DI*DI*WRAT2))
C SELECT U(R)D(R).
      DO 920 J=1,NS
      IF (ITEMPR .GT.MR(J)) GO TO 920
      URDR=1.0E-09*(A(J)*ITEMPR+B(J))
      BUBBLE=URDR/(ITEMPR*ITEMPR*1.0E-12)
      GO TO 927
  920 CONTINUE
C IF FALLS THROUGH HERE, WE HAVE GONE TOO FAR.
  925 WRITE(6,926)
  926 FORMAT(' ERROR ON SEGMENT RADIUS.')
      STOP
C WRITE RESULT FOR EACH I.
  927 IF (K.NE.1) GO TO 940
      WRITE(6,930) L,ITEMPR,WZI,URDR
  930 FORMAT(2X,I6,6X,I6,6X,E16.8,2X,E16.8)
  940 ITEMPR=ITEMPR+IDR
      SUM=SUM+(BUBBLE*BATH)
 1000 CONTINUE
C NOW CALCULATE SOUND VELOCITY.
      CNEW=1.0/((1.0/CZ)+((3.0*CZ*SUM)/(8.0*PI*PI*WW*WW*
     11.0E06)))
      CC(K)=CNEW-CZ
      WRITE(6,1010) ITEMPW,SUM,CNEW,CC(K)
 1010 FORMAT(' W = ',I6,4X,'SUM = ',E16.8,2X,'C = ',E16.8,
     12X,'DIFF = ',E16.8)
C PREPARE FOR NEXT ROUND OF W.
      ITEMPW=ITEMPW+IDW
 2000 CONTINUE
C ALL DONE..NOW PLOT W AND C.
      WRITE(6,2100)
 2100 FORMAT('1 RESULT:  W VS. (C-C0)')
      WRITE(6,2200)(W(I),CC(I),I=1,IW)
 2200 FORMAT(10X,E20.10,10X,E20.10)
      WRITE(6,2300)
 2300 FORMAT('1')
      CALL PLOTP (W,CC,IW,0)
      STOP
      END
```

BIBLIOGRAPHY

1. Buxcey, S., McNeil, J. E., Marks, R. H., Acoustic Detection of Microbubbles and Particulate Matter Near the Sea Surface, Thesis Naval Postgraduate School, Monterey, 1965.

2. Carlson, A. B., Communication Systems, Chapter 4, McGraw-Hill, 1968.

3. Fox, F. E., Curley, St. R., Larson, G. S., "Phase Velocity and Absorption Measurements in Water Containing Air Bubbles," Journal of the Acoustical Society of America, v. 27, No. 3, p. 534-539, May 1955.

4. Glotov, V. P., Kolobaev, P. A., Neuimin, G. G., "Investigation of the Scattering of Sound by Bubbles Generated by an Artificial Wind in Sea Water and the Statistical Distribution of Bubble Sizes," Soviet Physics-Acoustics, v. 7, No. 4, p. 341-345, April/June 1962.

5. Medwin, H., "In-Situ Acoustic Measurements of Bubble Population in Coastal Ocean Waters," Journal of Geophysical Research, v. 75, No. 3, p. 599-611, January 1970.

6. Meyer, E. Skudrzyk, Sound Absorption and Sound Absorbers in Water, NAV SHIPS 900.164, v. 1, 1 December 1950.

7. Truell, R., Elbaum, Ch., Chick, B. B., Ultrasonic Methods in Solid State Physics, Academic Press, 1969.

INITIAL DISTRIBUTION LIST

		No. Copies
1.	Defense Documentation Center Cameron Station Alexandria, Virginia 22314	2
2.	Library, Code 0212 Naval Postgraduate School Monterey, California 93940	2
3.	Commander, Naval Ordnance Systems Command Department of the Navy Washington, D. C. 20360	1
4.	Professor H. Medwin, Code 61Md Department of Physics Naval Postgraduate School Monterey, California 93940	10
5.	Assoc. Professor W. W. Denner, Code 58Dw Department of Oceanography Naval Postgraduate School Monterey, California 93940	1
6.	Asst. Professor E. B. Thornton, Code 58Tm Department of Oceanography Naval Postgraduate School Monterey, California 93940	1
7.	Asst. Professor N. E. Boston, Code 58Bb Department of Oceanography Naval Postgraduate School Monterey, California 93940	1
8.	Asst. Professor A. Eller, Code 61 Department of Physics Naval Postgraduate School Monterey, California 93940	1
9.	Asst. Professor G. Garrettson Department of Physics Naval Postgraduate School Monterey, California 93940	1
10.	LCDR Juergen Rautmann, FGN U -Bootslehrgruppe 243 Neustadt/Holstein Germany	3

		No. Copies
11.	Mr. William Smith Department of Physics Naval Postgraduate School Monterey, California 93941	1
12.	Commander, Naval Ship Systems Command ATTN: Code 00V1K Department of the Navy Washington, D. C. 20305	2
13.	Commander, U. S. Naval Oceanographic Office ATTN: Code 037-B Washington, D. C. 20390	1
14.	Director Acoustic Programs (Code 468 Office of Naval Research Department of the Navy Arlington, Virginia 22217	1

Security Classification

DOCUMENT CONTROL DATA - R & D

(Security classification of title, body of abstract and indexing annotation must be entered when the overall report is classified)

ORIGINATING ACTIVITY (Corporate author)

Naval Postgraduate School
Monterey, California 93940

2a. REPORT SECURITY CLASSIFICATION

Unclassified

2b. GROUP

REPORT TITLE

Sound Dispersion and Phase Fluctuations in the Upper Ocean

DESCRIPTIVE NOTES (Type of report and inclusive dates)

Master's Thesis; December 1971

AUTHOR(S) (First name, middle initial, last name)

Jürgen Rautmann

REPORT DATE	7a. TOTAL NO. OF PAGES	7b. NO. OF REFS
December 1971	92	7

8a. CONTRACT OR GRANT NO.	9a. ORIGINATOR'S REPORT NUMBER(S)
b. PROJECT NO.	
c.	9b. OTHER REPORT NO(S) (Any other numbers that may be assigned this report)
d.	

10. DISTRIBUTION STATEMENT

Approved for public release; distribution unlimited.

11. SUPPLEMENTARY NOTES	12. SPONSORING MILITARY ACTIVITY
	Naval Postgraduate School Monterey, California 93940

13. ABSTRACT

In-Situ measurements of the speed of sound in the upper ocean have revealed the existence of significant dispersion and large fluctuations over the frequency range 25-80 kHz. The near-surface values of c ranged from +6 M/sec to -3 M/sec relative to the bubble-free value, with a maximum estimated error of 0.5 M/sec. It was possible to identify bubbles of "surface" radius centered around 54 microns down to 4.3 meter depth as well as a population centered around 124 microns (at 4.3 M) found at all depths. The speed fluctuation showed near-Gaussian probability density functions except at the dispersion center frequencies. The standard deviation of the speed varied from 0.27 M/sec for 58.0 kHz to 0.52 M/sec at 69.6 kHz. The phase remained temporally correlated only for 1.46 sec., which was very close to the correlation times of the oceanographic variables. The power spectral density of the varying phase showed its strongest values at frequencies less than 0.5 Hz.; this was presumably due to bubbles entrained at orbital frequencies associated with the surface wave system which had maximum energy in the same frequency range.

DD FORM 1 NOV 65 1473 (PAGE 1)

S/N 0101-807-6811

Security Classification

A-31408

KEY WORDS	LINK A		LINK B		LINK C	
	ROLE	WT	ROLE	WT	ROLE	WT
Speed of sound						
Dispersion						
Phase fluctuations						
Bubbles						
Upper ocean						

29 JUL 76
BINDERY
2 a 3 u 2

132983
Thesis
R2454 Rautmann
c.1 Sound dispersion and phase fluctuations in the upper ocean.

BINDERY
2 a 3 u 2
29 JUL 76

132983
Thesis
R2454 Rautmann
c.1 Sound dispersion and phase fluctuations in the upper ocean.

thesR2454
Sound dispersion and phase fluctuations
3 2768 002 05317 5
DUDLEY KNOX LIBRARY